

## ANESTHESIOLOGY

# A Central Amygdala–Ventrolateral Periaqueductal Gray Matter Pathway for Pain in a Mouse Model of Depression-like Behavior

Weiwei Yin, M.S., Lisheng Mei, M.S., Tingting Sun, Ph.D., Yuping Wang, Ph.D., Jie Li, M.S., Changmao Chen, M.S., Zahra Farzinpour, M.D., Yu Mao, M.S., Wenjuan Tao, Ph.D., Juan Li, M.D., Wen Xie, M.D., Zhi Zhang, Ph.D.

ANESTHESIOLOGY 2020; 132:1175–96

## EDITOR'S PERSPECTIVE

### What We Already Know about This Topic

- Patients with depression are more likely to develop chronic pain and *vice versa*.
- Neuroimaging studies reveal that many brain regions implicated in depression also contribute to central pain processing.
- The mechanisms through which depressive states influence pain processing are poorly understood.

### What This Article Tells Us That Is New

- Chemogenetic experiments in a mouse model of depression reveal the involvement of a neural circuitry between the central amygdala and the periaqueductal gray in nociception.
- In this mouse model, pathologically increased activity of inhibitory  $\gamma$ -aminobutyric acid–mediated neurons in the central amygdala will result in the inhibition of inhibitory  $\gamma$ -aminobutyric acid–mediated neurons in the periaqueductal gray. This, in turn, will lead to the activation of glutamatergic cells involved in periaqueductal gray–mediated nociception.
- These findings provide a framework for how the central amygdala–periaqueductal gray circuitry may play a role in coping with nociception in depressive states.

## ABSTRACT

**Background:** The mechanisms underlying depression-associated pain remain poorly understood. Using a mouse model of depression, the authors hypothesized that the central amygdala–periaqueductal gray circuitry is involved in pathologic nociception associated with depressive states.

**Methods:** The authors used chronic restraint stress to create a mouse model of nociception with depressive-like behaviors. They then used retrograde tracing strategies to dissect the pathway from the central nucleus of the amygdala to the ventrolateral periaqueductal gray. The authors performed optogenetic and chemogenetic experiments to manipulate the activity of this pathway to explore its roles for nociception.

**Results:** The authors found that  $\gamma$ -aminobutyric acid–mediated (GABAergic) neurons from the central amygdala project onto GABAergic neurons of the ventrolateral periaqueductal gray, which, in turn, locally innervate their adjacent glutamatergic neurons. After chronic restraint stress, male mice displayed reliable nociception (control, mean  $\pm$  SD:  $0.34 \pm 0.11$  g,  $n = 7$  mice; chronic restraint stress,  $0.18 \pm 0.11$  g,  $n = 9$  mice,  $P = 0.011$ ). Comparable nociception phenotypes were observed in female mice. After chronic restraint stress, increased circuit activity was generated by disinhibition of glutamatergic neurons of the ventrolateral periaqueductal gray by local GABAergic interneurons *via* receiving enhanced central amygdala GABAergic inputs. Inhibition of this circuit increased nociception in chronic restraint stress mice (median [25th, 75th percentiles]:  $0.16$  [0.16, 0.16] g to  $0.07$  [0.04, 0.16] g,  $n = 7$  mice per group,  $P < 0.001$ ). In contrast, activation of this pathway reduced nociception (mean  $\pm$  SD:  $0.16 \pm 0.08$  g to  $0.34 \pm 0.13$  g,  $n = 7$  mice per group,  $P < 0.001$ ).

**Conclusions:** These findings indicate that the central amygdala–ventrolateral periaqueductal gray pathway may mediate some aspects of pain symptoms under depression conditions.

(ANESTHESIOLOGY 2020; 132:1175–96)

Pain and depression frequently coexist, rendering patients more difficult to treat.<sup>1,2</sup> In addition, depression may lead to a higher intensity of pain,<sup>3</sup> which tends to create a cycle of depression and pain that is difficult to break. To date, the underlying mechanisms of pain symptoms in depression are poorly understood.

Accumulating evidence from studies regarding brain networks,<sup>4,5</sup> neurotransmitter systems,<sup>6–8</sup> neuroplasticity,<sup>9–11</sup> and antidepressants<sup>12</sup> has revealed the common pathophysiologic mechanism. Neuroimaging studies show that numerous brain regions, such as the thalamus, amygdala, anterior cingulate cortex, prefrontal cortex, and insular cortex, are involved in the central mechanisms of depression.<sup>13,14</sup> Most of these

This article is featured in "This Month in Anesthesiology," page 1A. Supplemental Digital Content is available for this article. Direct URL citations appear in the printed text and are available in both the HTML and PDF versions of this article. Links to the digital files are provided in the HTML text of this article on the Journal's Web site ([www.anesthesiology.org](http://www.anesthesiology.org)). This article has a video abstract. This article has a visual abstract available in the online version. W.Y. and L.M. contributed equally to this article.

Submitted for publication May 13, 2019. Accepted for publication December 17, 2019. Published online first on January 27, 2020. From the Hefei National Laboratory for Physical Sciences at the Microscale, Key Laboratory of Brain Function and Disease of Chinese Academy of Science, Department of Biophysics and Neurobiology, University of Science and Technology of China, Hefei, China (W.Y., L.M., T.S., Y.W., Jie Li, C.C., Z.F., Y.M., W.T., Juan Li, Z.Z.); the Department of Psychology, Anhui Mental Health Center, Hefei, China (W.X., Z.Z.); and the Department of Physiology, School of Basic Medical Sciences, Anhui Medical University, Hefei, China (Y.M., W.T.).

Copyright © 2020, the American Society of Anesthesiologists, Inc. All Rights Reserved. Anesthesiology 2020; 132:1175–96. DOI: 10.1097/ALN.0000000000003133

brain regions are part of the descending pain modulatory system, which contributes to pain processing.<sup>15</sup> However, whether and how depression may influence the nociceptive system, which would further modify the central mechanisms of chronic pain, is still poorly understood. The brain regions involved in chronic pain closely mirror those involved in pain regulation, such as the amygdala, prefrontal cortex, and insular cortex.<sup>16,17</sup> In particular, the descending pain modulatory system is important for antidepressant action for pain relief.<sup>18</sup> Current antidepressants, such as serotonin reuptake inhibitors, target the descending pain system, and approximately one third of depression patients do not respond well to the treatment.<sup>19</sup> Some antidepressants may produce early adverse events in some patients, possibly further exacerbating pain symptoms.<sup>20,21</sup> Therefore, depression and pain are closely associated, but the mechanism—especially how the two are linked on the neuroanatomical and molecular substrate levels—is not yet understood.

Dysfunction of the descending pain inhibitory system is thought to be associated with pain in depression.<sup>22</sup> The amygdaloid complex, which is mainly composed of the basolateral amygdala and central amygdala,<sup>23</sup> is well known to modulate pain sensation, antinociception, and emotion processing.<sup>16,24,25</sup> Imaging studies have shown clinically significant alterations in the volume and activity of the amygdala in both depression and chronic pain patients.<sup>26–29</sup> Furthermore, the aforementioned prefrontal cortex and insular cortex have been reported to interact with the amygdala in processing cognition, emotion, and pain.<sup>30,31</sup> This raises the possibility that the amygdala could be an important site processing the pain symptoms of depression.

The central amygdala serves as the main output nucleus for amygdala functions.<sup>32</sup> Many studies have reported that the central amygdala is part of a descending endogenous pain control system that includes circuits in the brainstem, such as the periaqueductal gray and spinal cord.<sup>15,25</sup> Increased volume and neuronal proliferation in the central amygdala have been found in chronic pain.<sup>33</sup> Furthermore, the central amygdala forms extensive connections with forebrain areas, which have been shown to mediate fear and mood disorders.<sup>23,34</sup> These findings suggest that the central amygdala could be the convergent point of depression and chronic pain. However, the causal relationship between the adaptation of central amygdala circuits and the pathology of pain in depression is unknown. Based on the evidence linking the central amygdala with both depression and pain, we hypothesized that the central amygdala–periaqueductal gray circuitry is involved in the pathologic causes of pain in depression states.

## Materials and Methods

### Animals

In all experiments, C57BL/6J, *GAD2-Cre*, *CaMKII-Cre*, *c-fos-tTA*, and *Ai9* (RCL-tdT) male and C57BL/6J

female mice (purchased from Charles River or Jackson Laboratories, China) at 8 to 14 weeks of age were used. Except during cannula surgery, the mice were housed five per cage in a colony with *ad libitum* access to water and food. They were maintained under a 12-h light/dark cycle (lights on from 7:00 AM to 7:00 PM) at a stable temperature (23 to 25°C). After surgery, mice were allowed to recover for 1 week before further experiments. The animal protocols were approved by the Care Committee of the University of Science and Technology of China (Hefei, China).

All mice were randomly assigned to the control and experimental groups and were tested in sequential order. To minimize the stress resulting from behavioral testing, we first performed the sucrose preference test and then Von Frey/Hargreaves test before the chronic restraint stress protocol. After the stress protocol, the sucrose preference test, Von Frey/Hargreaves test, and forced swim/tail suspension test were conducted in sequential order. Behavioral tests were performed in the afternoon between 2:00 PM and 5:00 PM. No animal used for behavioral experiments was reused for other assays. A total of 350 mice were recruited for viral tracing, immunohistochemistry staining, and electrophysiologic and behavioral experiments in the current study. Of the mice used, 34 mice were excluded due to death or missed targets, including the injection of viruses and placement of optic fibers. The viral tracing and behavioral data were excluded from further analyses once it was found that these targets were missed. At the end of the experiments, mice were euthanized using carbon dioxide asphyxiation under isoflurane anesthesia.

### Chronic Restraint Stress

Mice were periodically constrained from moving by placing them in a 50-ml syringe for 6 h (between 11:00 AM and 5:00 PM) every day for 3 weeks without food or water. Holes were drilled in the ends of the syringes to allow the mice to breathe. During the restraint period, the control mice were allowed to move around freely in their original cages, but no food and water were provided. The syringes were thoroughly washed every day after the restraint period. The *c-fos-tTA* mice were perfused 90 min after the end of chronic restraint stress for immunofluorescence involving c-Fos expression and statistics. To exclude the effect of acute stress, the mice that underwent chronic restraint stress were allowed to rest 1 day before the anatomical and electrophysiologic experiments were conducted. In response to peer review, additional experiments pertaining to chronic restraint stress for the expression pattern and quantification of c-Fos in the mice brain regions were added.

### Spared Nerve Injury

The spared nerve injury surgery was performed under anesthesia with isoflurane. The skin and muscle of the left thigh were incised to explore the sciatic nerve, consisting of the sural, common peroneal, and tibial nerves. After

exploration, nonabsorbent 4-0 chromic gut sutures were used to ligate the common peroneal and tibial nerves, and then the nerves were transected, and about 2-mm sections from the dot were removed. The skin was stitched and disinfected with iodophor. For the sham mice, the procedure was the same as for the experimental group except that the nerves were left intact.

## Viral Injection

Mice were fixed in a stereotactic frame (RWD, China) under a combination of xylazine (10 mg/kg) and ketamine (100 mg/kg) anesthesia. A heating pad was used to maintain the core body temperature of the animals at 36°C. A volume of 60 to 250 nl virus (depending on the expression strength and viral titer) was injected using calibrated glass microelectrodes connected to an infusion pump (Micro4, WPI, USA) at a rate of 20 nl/min. The coordinates were defined as dorsal-ventral from the brain surface, anterior-posterior from the bregma, and medio-lateral from the midline (in mm).

For monosynaptic anterograde tracing, AAV-CMV-bG1-Cre-EGFP (AAV-Cre-eGFP, AAV2/1,  $2.79 \times 10^{13}$  vg/ml, 200 nl; Taitool, China) was injected into the amygdala (anterior-posterior: -1.0 mm, medio-lateral: -2.9 mm, dorsal-ventral: -3.85 mm) of C57BL/6J mice. After 3 weeks, mice that had been anesthetized with isoflurane followed by pentobarbital (20 mg/kg, intraperitoneal) were transcardially perfused, and brain slices were prepared (40  $\mu$ m) for tracing green fluorescent protein. In response to peer review, additional experiments pertaining to viral tracing for the projections from central amygdala to other brain regions were added.

For retrograde monosynaptic tracing, helper viruses that contained rAAV-Efl $\alpha$ -DIO-RVG-WPRE-pA (AAV-DIO-RVG, AAV2/9,  $2 \times 10^{12}$  vg/ml) and rAAV-Efl $\alpha$ -DIO-EGFP-2a-TVA-WPRE-pA (AAV-DIO-TVA-GFP, AAV2/9,  $2 \times 10^{12}$  vg/ml; 1:1, 60 nl) were coinjected into the ventrolateral periaqueductal gray (anterior-posterior: -4.72 mm; medio-lateral: -0.5 mm; dorsal-ventral: -2.0 mm) of *GAD2-Cre* and *CaMKII-Cre* animals. After 3 weeks, the rabies virus RV-EnvA- $\Delta$ G-dsRed ( $2 \times 10^8$  infectious units/ml, 100 nl) was injected into the same site of the ventrolateral periaqueductal gray. Mice that had been anesthetized with isoflurane followed by pentobarbital (20 mg/kg, intraperitoneal) were transcardially perfused 7 days after the last injection, and brain slices were prepared (40  $\mu$ m) for tracing discosoma species red fluorescent signal or costaining with  $\gamma$ -aminobutyric acid (GABA) antibody. The retrograde tracer cholera toxin B subunit conjugated with Alexa Fluor 555 (CTB-555, 0.1% w/v, 60 nl, ThermoLife, USA) was injected into the ventrolateral periaqueductal gray of C57BL/6J mice for 4 weeks to label ventrolateral periaqueductal gray-projecting central amygdala  $\gamma$ -aminobutyric acid-mediated (GABAergic) neurons for visualized electrophysiologic recordings.

The Cre-dependent virus rAAV-Efl $\alpha$ -DIO-hChR2 (H134R)-mCherry-WPRE-pA (AAV-DIO-ChR2-mCherry, AAV2/9,  $1.63 \times 10^{13}$  vg/ml, 200 nl) was delivered into the central amygdala (anterior-posterior: -1.0 mm, medio-lateral: -2.73 mm, dorsal-ventral: -3.75 mm) of *GAD2-Cre* mice. After 3 weeks, the expression of mCherry was detected in the whole brain. For the electrophysiologic exploration of central amygdala-ventrolateral periaqueductal gray pathway, the Cre-dependent virus rAAV-Efl $\alpha$ -DIO-hChR2 (H134R)-eYFP-WPRE-pA (AAV-DIO-ChR2-eYFP, AAV2/9,  $5 \times 10^{12}$  vg/ml, 200 nl) was injected into the central amygdala, and rAAV-Efl $\alpha$ -DIO-BFP-2a-TVA-WPRE-pA (AAV-DIO-BFP, AAV2/9,  $6 \times 10^{12}$  vg/ml, 150 nl) or rAAV-CaMKIIa-mCherry-WPRE-pA (AAV-CaMKIIa-mCherry,  $1.0 \times 10^{12}$  vg/ml, 150 nl) was infused into the ipsilateral ventrolateral periaqueductal gray of *GAD2-Cre* mice. AAV-DIO-ChR2-eYFP (150 nl) and AAV-CaMKIIa-mCherry (150 nl) were injected into the ventrolateral periaqueductal gray using the same coordinates for electrophysiologic study of the ventrolateral periaqueductal gray local microcircuit. In some experiments, rAAV-Efl $\alpha$ -DIO-eNpHR3.0-EYFP-WPRE-pA (AAV-DIO-eNpHR3.0-EYFP, AAV2/9,  $1.18 \times 10^{13}$  vg/ml, 250 nl) was used for optogenetic manipulation. The rAAV-Efl $\alpha$ -DIO-hM4D(Gi)-mCherry-WPRE-pA (AAV-DIO-hM4Di, AAV2/9,  $1.1 \times 10^{12}$  vg/ml; Hanbio, China) and rAAV-Efl $\alpha$ -DIO-hM3D(Gq)-mCherry-WPRE-pA (AAV-DIO-hM3Dq, AAV2/9,  $1.0 \times 10^{12}$  vg/ml; Hanbio) viruses were used for chemogenetic manipulations 4 weeks after viral injection, with intraperitoneal injection of clozapine-N-oxide (3 mg/kg, Sigma-Aldrich, USA) 30 min before the behavior test. To specifically manipulate the ventrolateral periaqueductal gray-projecting central amygdala neurons, AAV<sub>2/2</sub>-Retro-CMV-bG1-Cre-EGFP virus (Retro-Cre-GFP,  $2.03 \times 10^{13}$  vg/ml, 100 nl; Taitool, China) was injected into the right ventrolateral periaqueductal gray, and a volume of 200 nl chemogenetic viruses was infused into the ipsilateral central amygdala of C57BL/6J mice. The rAAV-Efl $\alpha$ -DIO-mCherry-WPRE-pA (AAV2/8,  $8.93 \times 10^{12}$  vg/ml) and rAAV-DIO-EYFP-WPRE-pA (AAV2/9,  $1.95 \times 10^{12}$  vg/ml) viruses were used as the controls. Unless otherwise stated, all viruses were packaged by BrainVTA (China). All mice were transcardially perfused with 0.9% saline followed by ice-cold phosphate buffer (0.1 M) that contained 4% paraformaldehyde. Images of the signal expression were acquired with a confocal microscope (LSM 710, Zeiss, Germany). Animals with missed injections were excluded.

## Brain Slice Electrophysiology

**Brain Slice Preparation.** Acute brain slices were prepared as previously described.<sup>35</sup> Mice were deeply anesthetized with isoflurane followed by intraperitoneal injection of pentobarbital sodium (2%, w/v, intraperitoneal) and intracardially perfused with ~20 ml ice-cold oxygenated modified

*N*-methyl-D-glucamine artificial cerebrospinal fluid that contained (in mM) 93 *N*-methyl-D-glucamine, 2.5 potassium chloride, 0.5 calcium chloride, 20 HEPES, 1.2 monosodium phosphate, 30 sodium bicarbonate, 10 magnesium sulphate, 25 glucose, 5 sodium ascorbate, 3 sodium pyruvate, 2 thiourea, and 3 glutathione (pH: 7.3 to 7.4, osmolality: 300 to 305 milliosmole/kg). Coronal slices (300  $\mu$ m) that contained the central amygdala or ventrolateral periaqueductal gray were sectioned with a vibrating microtome (VT1200 S, Leica) and were initially incubated in HEPES artificial cerebrospinal fluid that contained (in mM) 2.5 potassium chloride, 92 sodium chloride, 1.2 monosodium phosphate, 30 sodium bicarbonate, 20 HEPES, 25 glucose, 2 thiourea, 5 sodium ascorbate, 3 sodium pyruvate, 3 glutathione, 2 calcium chloride, and 2 magnesium sulphate (pH: 7.3 to 7.4, osmolality: 300 to 305 milliosmole/kg) for at least 1 h at 25°C. The brain slices were transferred to a slice chamber (Warner Instruments, USA) with artificial cerebrospinal fluid perfusion at 2.5 to 3 ml/min at 32°C for electrophysiologic recording; the temperature of the artificial cerebrospinal fluid was maintained by an in-line solution heater (TC-344B, Warner Instruments).

**Whole Cell Patch-clamp Recordings.** Neurons were visualized using a 40 $\times$  water immersion objective on an upright microscope (BX51WI, Olympus, Japan) equipped with interference contrast (infrared differential interference contrast optics) and an infrared camera connected to the video monitor. Whole cell patch-clamp recordings were obtained from visually identified central amygdala or ventrolateral periaqueductal gray cells. Patch pipettes (3 to 5 M $\Omega$ ) were pulled from borosilicate glass capillaries (VitalSense Scientific Instruments Co., Ltd., China) with an outer diameter of 1.5 mm on a four-stage horizontal puller (P1000, Sutter Instruments, USA). The signals were acquired *via* a MultiClamp 700B amplifier, low-pass-filtered at 2.8 kHz, digitized at 10 kHz, and analyzed with Clampfit 10.7 software (Molecular Devices, USA). The data were collected from the neurons with series resistance less than 30 M $\Omega$  and input resistance greater than 100 M $\Omega$ . In some experiments, 0.5% neurobiotin 488 was included in the intracellular solution, together with immunofluorescence staining, for cell type identification. The current-evoked firing was recorded in current-clamp mode ( $I = 0$  pA). The threshold current for firing was defined as the minimum strength of current injection required to elicit at least one or two spikes. For recording the intrinsic membrane properties, the pipettes (5 to 7 M $\Omega$ ) were filled with potassium gluconate-based internal solution containing (in mM) 130 potassium gluconate, 2 magnesium chloride, 5 potassium chloride, 0.6 EGTA, 10 HEPES, 2 magnesium-adenosine triphosphate, and 0.3 sodium guanosine 5'-triphosphate sodium salt hydrate (osmolality: 285 to 290 milliosmole/kg, pH: 7.2). Measurement of the intrinsic membrane properties was conducted under current-clamp mode, and data were collected from neurons with a resting membrane potential

less than  $-50$  mV and an overshoot of the action potentials. Spontaneous miniature inhibitory postsynaptic currents were recorded in the presence of glutamate receptor antagonists D-(–)-2-amino-5-phosphonopentanoic acid (50  $\mu$ M), 6-cyano-7-nitroquinoxaline-2,3-dione (10  $\mu$ M), and sodium channel blocker tetrodotoxin (1  $\mu$ M). The frequency and amplitude of miniature inhibitory postsynaptic currents were analyzed by a sliding inhibitory postsynaptic current template custom-defined with the acquisition software. The threshold current of the action potential was defined as the minimum current to elicit an action potential.

In response to peer review, additional experiments pertaining to electrophysiologic recording of the firing rate of ventrolateral periaqueductal gray-projecting central amygdala GABAergic neurons in a mouse model of neuropathic pain, and the miniature inhibitory postsynaptic currents of ventrolateral periaqueductal gray GABAergic and glutamatergic neurons, were added.

**Light-evoked Response.** Optical stimulation was delivered using a laser (Shanghai Fiblaser Technology Co., Ltd., China) through an optical fiber 200  $\mu$ m in diameter positioned 0.2 mm from the surface of the brain slice. To test the functional characteristics of AAV-DIO-ChR2-mCherry, fluorescently labeled neurons that expressed channelrhodopsin-2 in *GAD2-Cre* mice 3 to 4 weeks after virus injection were visualized and stimulated with a blue (473 nm, 5 to 10 mV) laser light using 5-Hz, 10-Hz, and 20-Hz stimulation protocols with a pulse width of 15 ms. In some experiments, the function of enhanced natronomonas pharaonis halorhodopsin 3.0 was assessed by applying sustained yellow (594 nm, 5 to 10 mV, 200 ms) laser light stimulation. For the recording of photostimulation-induced inhibitory postsynaptic currents, cells were recorded at 0 mV after photostimulation (10 mW, 10 ms) of channelrhodopsin-2-expressing fibers in the ventrolateral periaqueductal gray slices. To block the  $\alpha$ -amino-3-hydroxy-5-methyl-4-isoxazole propionic acid receptors, 10  $\mu$ M 6,7-dinitroquinoxaline-2,3-dione was added into the standard artificial cerebrospinal fluid. Pipettes were filled with the aforementioned potassium gluconate-based internal solution. In response to peer review, an additional three samples pertaining to electrophysiologic recording of optical stimulation-elicited inhibitory postsynaptic currents in ventrolateral periaqueductal gray GABAergic neurons were added.

### Immunohistochemistry and Imaging

The mice were deeply anesthetized with isoflurane followed by intraperitoneal injection of pentobarbital sodium (50 mg/kg, intraperitoneal) and sequentially perfused with saline and 4% (w/v) paraformaldehyde. The brains were subsequently removed and postfixed in 4% paraformaldehyde at 4°C overnight. After cryoprotection of the brains with 30% (w/v) sucrose, coronal sections (40  $\mu$ m) were cut on a cryostat (CM1860, Leica) and used for immunofluorescence. The sections were incubated in 0.3% (v/v) Triton

X-100 for 0.5 h, blocked with 10% donkey serum for 1 h at room temperature, and incubated with primary antibodies, including anti-GABA (1:500, rabbit; Sigma-Aldrich, catalog No. A2052, RRID: AB\_477652) and anti-glutamate (1:500, rabbit; Sigma-Aldrich, catalog No. G6642, RRID: AB\_259946), at 4°C for 24 h, followed by Alexa 488-conjugated (1:500, Invitrogen; catalog No. A21206) or Alexa 647-conjugated (1:500, Invitrogen; catalog No. A31573) secondary antibodies for 2 h at room temperature. Fluorescence signals were visualized using a Zeiss LSM710 microscope. For *post hoc* immunofluorescence, slices were collected after whole cell recording, in which the patched neurons were labeled with neuronbictin-488 and were immersed into 4% paraformaldehyde for postfixation at 4°C for 1 week. Then, slices were washed in 0.01 M phosphate-buffered saline for  $3 \times 30$  min, followed by incubation overnight with blocking solution (10% [v/v] donkey serum, 1.0% [v/v] Triton X-100 dissolved in 0.01 M phosphate-buffered saline). Then, slices were incubated with primary antibody diluted in blocking solution at 4°C for 3 days, including anti-GABA (1:100, rabbit; Sigma-Aldrich, catalog No. A2052, RRID: AB\_477652). After washing in 0.01 M phosphate-buffered saline, slices were immersed in Alexa 647-conjugated secondary antibody (1:100, Invitrogen catalog No. A31573) diluted in 0.01 M phosphate-buffered saline at room temperature for 8 h and then washed in 0.01 M phosphate-buffered saline for  $3 \times 30$  min and mounted on the glass slides. Images were captured *via* confocal microscopy. For the identification of c-Fos-positive or rabies and fluorescent protein-labeled ventrolateral periaqueductal gray-projecting central amygdala neurons, 2 or 3 slices per mouse from the coordinate of  $-1.06$ ,  $-1.34$ , or  $-1.46$  in the anterior-posterior direction were chosen; for the identification of c-Fos-positive ventrolateral periaqueductal gray neurons, 2 or 3 slices per mouse from the coordinate of  $-4.48$ ,  $-4.60$ , or  $-4.72$  in the anterior-posterior direction were chosen according to *The Mouse Brain in Stereotaxic Coordinates*.<sup>36</sup> Then images containing central amygdala and ventrolateral periaqueductal gray were captured under a 20 $\times$  objective, 0.18 mm<sup>2</sup> (the full field of view) and 0.016 mm<sup>2</sup> imaging area per slice for central amygdala and ventrolateral periaqueductal gray analysis, respectively. To avoid experimenter bias, the images were randomly renamed with Arabic numerals and analyzed by an assessor blind to the experimental conditions.

### Assessment of Depressive-like Behaviors

Mice were transported to the behavioral testing room in a holding cabinet to habituate at least 2 h before testing. The behavior of the animals during testing was recorded using a video tracking system and was subsequently analyzed offline. Dim light ( $\sim 20$  lux) was used in the room to minimize the anxiety of the animals.

**Forced Swim Test.** A mouse was placed in a transparent Plexiglas cylinder (30 cm high and 12 cm in diameter)

that contained fresh water ( $24 \pm 1^\circ\text{C}$ ) up to a height of 25 cm from the bottom for 6 min. The animal's behavior was videotaped from the side, and the duration of immobility of each mouse during the last 5 min of recording was measured offline. Mice from the control and experimental groups were tested in alternate order. A mouse was considered immobile when remaining motionless or floating. The copies of video files were randomly renamed by the investigator with Arabic numerals and then manually analyzed by an assessor blind to the assignment. In response to peer review, additional experiments pertaining to forced swim tests for depression-like behaviors after chemogenetic manipulations of ventrolateral periaqueductal gray-projecting central amygdala neurons were added.

**Sucrose Preference Test.** Mice were singly housed and habituated with two identical bottles of 1% sucrose for 2 days followed by 2 days of water. Then the experimental mice were water-deprived for 24 h. After that, the mice were presented with two bottles for 2 h, one containing water and the other containing 1% sucrose, and the positions were switched after 1 h. The consumption of each fluid was measured, and sucrose preferences were calculated as follows:  $\Delta\text{weight of sucrose water} / (\Delta\text{weight of sucrose water} + \Delta\text{weight of water}) \times 100$ . In response to peer review, additional experiments pertaining to sucrose preference tests for the depression-like behaviors during optical manipulations of the central amygdala GABAergic terminals in the ventrolateral periaqueductal gray, and sucrose preference tests for depression-like behaviors after chemogenetic manipulations of ventrolateral periaqueductal gray-projecting central amygdala neurons, were added.

**Tail Suspension Test.** Mice were individually suspended by their tails with tape in the rectangular compartment (55 height  $\times$  20 width  $\times$  11.5 cm depth) of a specially manufactured two-walled tail suspension box (55 height  $\times$  40 width  $\times$  11.5 cm depth). Mice were considered immobile without initiated movements, and immobility was considered to include passive swaying. In response to peer review, additional experiments pertaining to tail suspension tests for the depression-like behaviors during optical manipulations of central amygdala GABAergic terminals in the ventrolateral periaqueductal gray were added.

### Nociceptive Tests

Nociceptive thresholds were measured on freely moving mice with Von Frey and Hargreaves tests.

**Von Frey Test.** Mice were placed in transparent plastic chambers individually on a wire mesh grid to allow calibrated Von Frey filaments inserting in the surface of the hind paw. Before testing, mice were allowed to accustom themselves to the testing environment for at least 30 min. A set of Von Frey monofilaments was used to test the mechanical hyperalgesia (with marking forces of 0.02, 0.04, 0.07, 0.16, 0.4, 0.6, and 1 g), the paw withdrawal thresholds were generated by placing continuous pressure on the plantar region of the

paws, each hind paw was measured five times with a 10-min interval, and the mean threshold was calculated from five applications. The mice with metal ear tags were randomly placed in chambers by the investigator, and the withdrawal threshold was tested by an assessor blind to the assignment. In response to peer review, additional experiments pertaining to Von Frey tests for mechanical nociception after optical activation of central amygdala GABAergic terminals in the ventrolateral periaqueductal gray in a mouse model of neuropathic pain, Von Frey tests for nociception in a female mouse model of depression-like behavior, and Von Frey tests for mechanical nociception of a nonchronic restraint stress control group were added.

**Hargreaves Test.** Mice were placed in transparent plastic chambers on a glass platform maintained at 30°C. A radiant heat beam was focused onto the left hind paw (IITC Life Science Inc., USA). The latency to hind paw withdrawal was recorded with 3 to 5 trials per animal at 10-min intervals. The beam intensity was adjusted to keep control mice displaying a latency of 10 to 15 s. A 30-s cutoff was set to avoid tissue damage. In response to peer review, additional experiments pertaining to Hargreaves tests for thermal nociception during optical manipulations of central amygdala GABAergic terminals in the ventrolateral periaqueductal gray, Hargreaves tests for thermal nociception in a female mouse model of depression-like behavior, Hargreaves tests for the thermal nociception of a nonchronic restraint stress control group, Hargreaves tests for the thermal nociception in a male mouse model of depression-like behavior, and Hargreaves tests for thermal nociception after chemogenetic manipulations of ventrolateral periaqueductal gray-projecting central amygdala neurons were added. In the last two Hargreaves tests, cohorts were used differently from those by Von Frey tests.

### Optogenetic Manipulations *In Vivo*

An optical fiber cannula was initially implanted over the ventrolateral periaqueductal gray of a pentobarbital sodium-anesthetized mouse that had been immobilized in a stereotaxic apparatus. The implant was secured to the animal's skull with dental cement. Chronically implantable fibers (diameter, 200  $\mu$ m, Newdoon, China) were connected to a laser generator using optic fiber sleeves. The delivery of a 6-s pulse of blue light (473 nm, 2 to 5 mW, 15-ms pulses, 20 Hz) or yellow light (594 nm, 5 to 8 mW, constant) was controlled by a Master-8 pulse stimulator (A.M.P.I., Israel). The same stimulus protocol was applied to the mice in the control group. The location of the fibers was examined in all mice at the conclusion of the experiments, and data obtained from mice in which the fibers were located outside of the desired brain region were discarded. The mechanical and thermal nociception tests were performed 3 s after blue light or every 5 min during the yellow light stimulation. For the test of depressive-like behaviors, mice were subjected to tail suspension for 1 min followed

by testing epochs of 3 min off/3 min on/3 min off, or mice were subjected to the sucrose preference test for 2 h after a 30-min photostimulation. To avoid the effect of freezing on the immobility time of the tail suspension test, the blue light intensity was adjusted to keep channelrhodopsin-2 group mice freely moving.

### Statistical Analysis

The quantile-quantile plots were used to verify the assumptions before the *t* test, ANOVA, and descriptive statistics by using SPSS statistical software (version 22; SPSS, Inc., USA). After the assumptions were verified, we conducted simple statistical comparisons using independent Student's *t* test. An ANOVA (one-way and two-way ordinary/repeated measures, between subjects) with a Bonferroni *post hoc* analysis was used to statistically analyze the data from the experimental groups with multiple comparisons. Otherwise, data were analyzed by a Mann-Whitney test or Wilcoxon matched-pairs signed-rank test. Two-tailed testing was used as per convention. No *a priori* statistical power calculation was conducted. The sample size was selected based on the available data. The parametric data are expressed as the mean  $\pm$  SD, and nonparametric data are presented as median (25th, 75th percentiles); outliers, if any, were always included in the analyses. The significance levels are indicated as \**P* < 0.05, \*\**P* < 0.01, and \*\*\**P* < 0.001. OriginPro 2017 software (OriginLab Corporation, USA) and GraphPad Prism 5 (GraphPad Software, Inc., USA) were used for the statistical analyses and graphing. Offline analysis of the data obtained from electrophysiologic recordings was conducted using Clampfit software version 10.7 (Axon Instruments, Inc., USA). All statistical data are presented in table S1 (Supplemental Digital Content, <http://links.lww.com/ALN/C172>).

## Results

### Chemogenetic Dissection of the Central Amygdala–Ventrolateral Periaqueductal Gray Circuit

We focused on the central amygdala–periaqueductal gray pathway because it is a critical relay in the descending pain inhibitory system, dysfunction of which may be associated with pain.<sup>1,37,38</sup> To characterize central amygdala–periaqueductal gray contacts, we first injected an anterograde transmonosynaptic virus that transported adeno-associated viruses, delivering a construct containing an enhanced green fluorescent protein tag (AAV-CMV-bG1-Cre-EGFP) into the mouse amygdala (fig. 1, A and B, left).<sup>39</sup> We found that the green fluorescent signal was mainly detected in the ipsilateral ventrolateral periaqueductal gray and parabrachial nucleus and was weakly detected in the dorsal raphe nucleus, lateral periaqueductal gray, and contralateral ventrolateral periaqueductal gray (ventrolateral periaqueductal gray:  $21 \pm 3$  cells/slice, parabrachial nucleus:  $21 \pm 6$  cells/

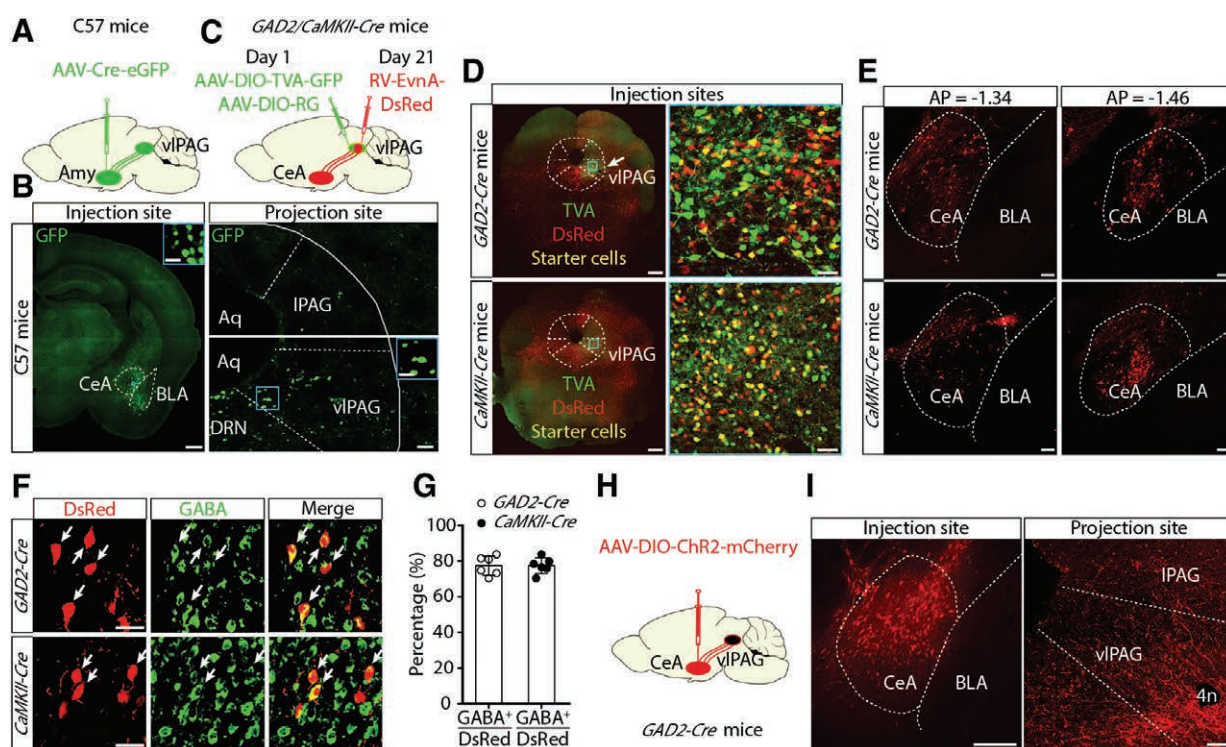


**Fig. 1.** The central amygdala (Amy)  $\gamma$ -aminobutyric acid-mediated (GABAergic) neurons projects onto ventrolateral periaqueductal gray neurons. (A) Schematic diagram of AAV-Cre-eGFP injected into the Amy for anterograde tracing. (B) *Left*, Viral expression in the Amy of a C57BL/6J mouse. Scale bar, 500  $\mu$ m; *inset*, 25  $\mu$ m. *Right*, A representative image of the projection site in ipsilateral lateral periaqueductal gray (*top*), ventrolateral periaqueductal gray, and dorsal raphe nucleus (*bottom*). Scale bar, 50  $\mu$ m; *inset*, 25  $\mu$ m. (C) Strategy for cell type-specific monosynaptic tracing. (D) Representative images of the viral injection site and expression within the ventrolateral periaqueductal gray. Starter cells (yellow) coexpressing TVA-GFP (*green*), rabies G and RV-EnvA- $\Delta$ G-dsRed (*red*) in ventrolateral periaqueductal gray of *GAD2-Cre* mice (*top*) and *CaMKII-Cre* (*bottom*) mice. Scale bar, 500  $\mu$ m; *inset*, 50  $\mu$ m. (E) Representative images of presynaptic cells in central Amy. Rabies-labeled cells within central Amy of *GAD2-Cre* mice (*top*) and *CaMKII-Cre* (*bottom*) mice. Numbers indicate the distance from bregma. Scale bar, 100  $\mu$ m. (F) Identification of rabies virus-labeled central Amy neurons. White arrows represent colocalization of rabies virus–discosoma species red fluorescent protein and  $\gamma$ -aminobutyric acid (GABA; *top*: rabies virus–positive cells and GABA, *GAD2-Cre* mouse; *bottom*: rabies virus–positive cells and GABA, *CaMKII-Cre* mouse). Scale bar, 25  $\mu$ m. (G) Quantitation of GABA-expressing rabies virus–positive cells that projection onto ventrolateral periaqueductal gray GABAergic and glutamatergic neurons ( $77.7\% \pm 5.4\%$  and  $77.7\% \pm 4.5\%$ ;  $n = 6$  slices from three mice per group). (H) Strategy for cell type-specific anterograde tracing. (I) Schematic showing the Chr2-expressing cells in central Amy and terminals in ventrolateral periaqueductal gray of *GAD2-Cre* mice. Scale bars, 200  $\mu$ m and 100  $\mu$ m, respectively. Aq, aqueduct; AP, anterior-posterior; BLA, basolateral amygdala; CeA, central amygdala; DRN, dorsal raphe nucleus; Chr2, channelrhodopsin-2; DsRed, discosoma species red fluorescent protein; IPAG, lateral periaqueductal gray; rabies G, rabies virus glycoprotein; RV, rabies virus; TVA, avian tumor virus receptor A; vIPAG, ventrolateral periaqueductal gray; 4n, trochlear nerve.

slice, dorsal raphe nucleus:  $14 \pm 2$  cells/slice, lateral periaqueductal gray:  $3 \pm 1$  cells/slice; fig. 1B, right; Supplemental Digital Content, fig. S1, <http://links.lww.com/ALN/C172>).

To further identify the cell type-specific connections between central amygdala and ventrolateral periaqueductal gray neurons, we used a Cre-dependent retrograde trans-monosynaptic tracing strategy to identify the type of ventrolateral periaqueductal gray neurons receiving central amygdala projections. Given that glutamatergic and GABAergic neurons are typical and dominant cells in the ventrolateral periaqueductal gray, the Cre-dependent helper viruses (AAV-Ef1 $\alpha$ -DIO-TVA-GFP

and AAV-Ef1 $\alpha$ -DIO-RVG) were injected into the ventrolateral periaqueductal gray of the  $Ca^{2+}$ /calmodulin-dependent protein kinase II (an enzyme in glutamatergic neurons)–Cre mice or glutamic acid decarboxylase 2 (a GABA-synthesizing enzyme)–Cre mice. After 3 weeks, the glycoprotein gene-defective recombinant rabies virus vectors expressing red fluorescent proteins (EnvA-pseudotyped RV- $\Delta$ G-DsRed) were injected into the same site and exclusively infected the helper virus–positive ventrolateral periaqueductal gray glutamatergic or GABAergic neurons with the help of envelope protein of avian sarcoma and leucosis virus.<sup>40</sup> The ventrolateral periaqueductal gray glutamatergic or GABAergic neurons expressing both green

and red fluorescent proteins were defined as starter cells because part of them was directly innervated by axons from central amygdala, and the presence of glycoprotein-expressing helper viruses enabled the glycoprotein gene-defective recombinant rabies virus to spread monosynaptically retrogradely (fig. 1, C and D).<sup>41</sup> We identified intensely discosoma species red fluorescent protein-labeled neurons in the central amygdala of *GAD2-Cre* and *CaMKII-Cre* mice (fig. 1E). The red fluorescent signal was mostly colocalized with the GABA antibody based on immunofluorescence staining (*GAD2-Cre*, 77.7%  $\pm$  5.4%; *CaMKII-Cre*, 77.7%  $\pm$  4.5%;  $n = 6$  slices from three mice per group; fig. 1, F and G). These results indicate that both ventrolateral periaqueductal gray GABAergic and glutamatergic neurons receive central amygdala GABAergic projections. To confirm this observation, an adeno-associated virus expressing Cre-dependent channelrhodopsin-2 (AAV-DIO-ChR2-mCherry) was infused into the central amygdala of the *GAD2-Cre* mice (fig. 1H). We observed mCherry<sup>+</sup> GABAergic cell bodies in the central amygdala and numerous mCherry<sup>+</sup> fibers in the ventrolateral periaqueductal gray as well as in other brain regions (fig. 1I; Supplemental Digital Content, fig. S2, <http://links.lww.com/ALN/C172>).

To characterize the functional connections of the central amygdala–periaqueductal gray pathway, we first injected the double-floxed Cre-dependent adeno-associated virus vector, delivering a construct that contained a blue fluorescent protein tag (AAV-DIO-BFP) or the  $Ca^{2+}$ /calmodulin-dependent protein kinase II promoter-dependent AAV-CaM-mCherry into the ventrolateral periaqueductal gray of *GAD2-Cre* mice to infect ventrolateral periaqueductal gray GABAergic or glutamatergic neurons, respectively; then AAV-DIO-ChR2-eYFP was injected into the central amygdala for visualized recording (fig. 2A). After 3 weeks, we observed dense perisomatic yellow fluorescent protein-positive fibers (GABA fibers) surrounding blue fluorescence protein-positive (GABA neurons) or red fluorescent protein-positive (glutamate neurons) cell bodies in the ventrolateral periaqueductal gray (fig. 2B). At 0 mV holding potentials, optical stimulation of channelrhodopsin-2-containing central amygdala GABAergic terminals in the ventrolateral periaqueductal gray reliably elicited inhibitory postsynaptic currents in ventrolateral periaqueductal gray GABAergic neurons in brain slices, which were blocked by the GABA receptor antagonist bicuculline (104.4  $\pm$  51.3 pA *vs.* 2.6 [1.9, 3.2] pA,  $n = 8$  cells from three mice per group,  $P = 0.008$ ; fig. 2, C and D). In contrast, ventrolateral periaqueductal gray glutamatergic neurons showed an increased action potential firing rate during optical activation of the central amygdala GABAergic terminal in the ventrolateral periaqueductal gray (0 [0, 1] spikes/s *vs.* 2 [1, 5] spikes/s,  $n = 8$  cells from three mice per group,  $P = 0.008$ ; fig. 2, E–H). This result may suggest a local inhibitory microcircuit within the ventrolateral periaqueductal gray (fig. 2I). To test this hypothesis, we injected the AAV-DIO-ChR2-eYFP

after AAV-CaM-mCherry into the ventrolateral periaqueductal gray of *GAD2-Cre* mice (fig. 2J). Photostimulation of ventrolateral periaqueductal gray GABAergic neurons reliably induced inhibitory postsynaptic currents in ventrolateral periaqueductal gray glutamatergic neurons, which were blocked by bicuculline (185.9  $\pm$  101.0 pA *vs.* 15.5  $\pm$  33.6 pA,  $n = 5$  cells from three mice per group,  $P = 0.016$ ; fig. 2, K and L). Of note, the amplitude of these inhibitory postsynaptic currents was much bigger than that induced by optical activation of central amygdala GABAergic terminals in the ventrolateral periaqueductal gray (185.9  $\pm$  101.0 pA *vs.* 104.4  $\pm$  51.3 pA,  $n = 5$  ventrolateral periaqueductal gray glutamatergic and 8 GABAergic cells from three mice per group). These results reveal a microcircuit organization wherein ventrolateral periaqueductal gray glutamatergic neurons are innervated by local inhibitory GABAergic interneurons, both of which receive direct central amygdala GABAergic inputs. Moreover, activation of central amygdala GABAergic neurons results in the disinhibition of ventrolateral periaqueductal gray glutamatergic neurons *via* local GABAergic neurons.

### Enhanced Excitability of the Central Amygdala–Ventrolateral Periaqueductal Gray Pathway in Mice Treated with Chronic Restraint Stress

To determine the role of the central amygdala–ventrolateral periaqueductal gray circuit in depression-related pain, we used a chronic restraint stress model in mice to induce depressive-like behaviors (fig. 3A; Supplemental Digital Content, fig. S3A, <http://links.lww.com/ALN/C172>). Chronic restraint stress, a classic method that is used to simultaneously induce psychologic and physiologic stress, can induce both depressive-like behaviors<sup>42–44</sup> and increased nociception<sup>45</sup> in mice. After the 3-week chronic restraint stress, both male and female mice displayed depressive-like behaviors in the sucrose preference test (*i.e.*, reduced sucrose consumption; male: day 14, 80.3%  $\pm$  11.5% *vs.* 65.2%  $\pm$  17.7%,  $P = 0.04$ ; day 21, 86.6%  $\pm$  7.3% *vs.* 61.0%  $\pm$  15.2%,  $P = 0.028$ ; female: day 21, 81.7%  $\pm$  10.1% *vs.* 59.3%  $\pm$  17.2%,  $P = 0.002$ ; fig. 3B; Supplemental Digital Content, fig. S3B, <http://links.lww.com/ALN/C172>) and forced swimming test (*i.e.*, increased immobility; male: day 24, 128.9  $\pm$  45.7 s *vs.* 175.1  $\pm$  33.4 s; female: day 24, 109.3  $\pm$  26.8 s *vs.* 157.6  $\pm$  37.9 s,  $P = 0.004$ ; fig. 3C; Supplemental Digital Content, fig. S3C, <http://links.lww.com/ALN/C172>), accompanied by a reduction in mechanical nociception threshold (male: day 23, 0.34  $\pm$  0.11 g *vs.* 0.13 [0.10, 0.25] g,  $n = 7$  control and 9 chronic restraint stress mice,  $P = 0.016$ ; female: day 23, 0.40 [0.40, 0.60] g *vs.* 0.16 [0.07, 0.16] g,  $n = 10$  control and 9 chronic restraint stress mice,  $P < 0.001$ ; fig. 3D; Supplemental Digital Content, fig. S3D, <http://links.lww.com/ALN/C172>); only male mice showed thermal hypersensitivity (day 23: 12.64  $\pm$  1.47 s *vs.* 10.91  $\pm$  1.44 s,  $n = 8$  mice per group,  $P = 0.032$ ; Supplemental Digital Content, fig. S3, E and F, <http://links.lww.com/ALN/C172>). Male

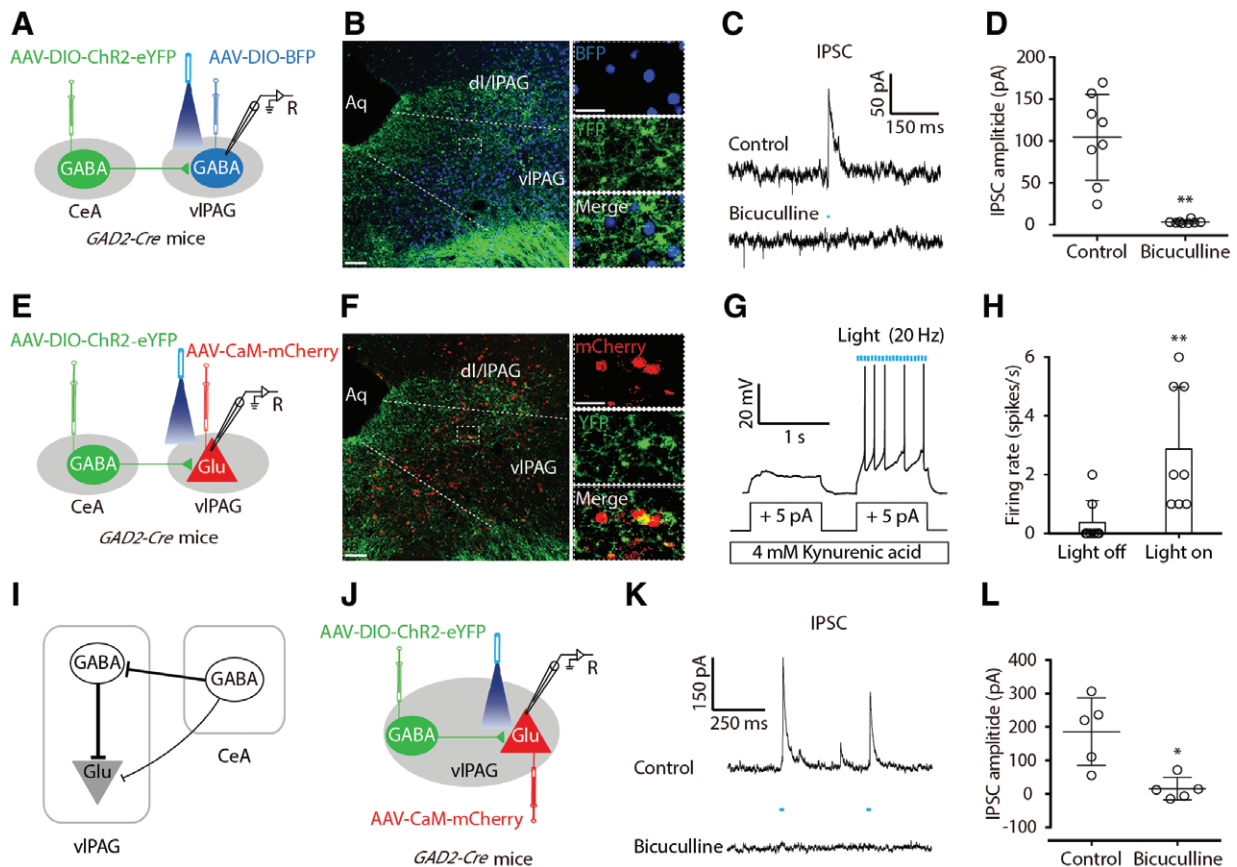


**Fig. 2.** A disinhibitory circuit from central amygdala  $\gamma$ -aminobutyric acid-mediated (GABAergic) neurons to ventrolateral periaqueductal gray glutamatergic neurons *via* local GABAergic neurons. (A) Schematic showing the strategy of expressing ChR2 in central amygdala GABAergic neurons and blue fluorescence protein in ventrolateral periaqueductal gray GABAergic neurons for targeted whole cell patch-clamp recordings. (B) ChR2 and blue fluorescence protein expression pattern in the ventrolateral periaqueductal gray of a *GAD2-Cre* mouse. Scale bar, 100  $\mu$ m; inset, 25  $\mu$ m. (C) Inhibitory postsynaptic currents recorded at 0 mV from a ventrolateral periaqueductal gray GABAergic neuron after 10 ms photostimulation of GABAergic fibers from central amygdala (top) was blocked after bath application of 10  $\mu$ M bicuculline (bottom). (D) Summarized data of the light-evoked inhibitory postsynaptic currents amplitude ( $n = 8$  cells from eight slices of three mice, two-tailed Wilcoxon matched-pairs signed rank test,  $P = 0.008$ ). (E) Schematic showing the strategy of expressing ChR2 in central amygdala  $\gamma$ -aminobutyric acid (GABA) and mCherry in ventrolateral periaqueductal gray glutamatergic neurons for targeted whole cell patch-clamp recordings. (F) ChR2 and mCherry expression pattern in the ventrolateral periaqueductal gray of a *GAD2-Cre* mouse. Scale bar, 100  $\mu$ m; inset, 25  $\mu$ m. (G) Light-evoked robust action potential firing (observed in all ventrolateral periaqueductal gray glutamatergic neurons tested) after the application of 4  $\mu$ M kynurenic acid to block glutamate at ionotropic receptors. (H) Quantitation of action potential firing rate before and after 10 ms photostimulation ( $n = 8$  cells from six slices of two mice, two-tailed Wilcoxon matched-pairs signed rank test,  $P = 0.008$ ). (I) Schematic illustration of central amygdala and GABA-ventrolateral periaqueductal gray pathway. (J) Expression of ChR2 in ventrolateral periaqueductal gray GABAergic and mCherry in glutamatergic neurons for targeted whole cell patch-clamp recordings. Scale bar, 10  $\mu$ m. (K) Light-evoked inhibitory postsynaptic currents (top) were blocked by 10  $\mu$ M bicuculline application (bottom). (L) Summarized data of 10 ms light-evoked inhibitory postsynaptic currents amplitude ( $n = 5$  cells from five slices of three mice, two-tailed paired Student's *t* test,  $t[4] = 3.98$ ,  $P = 0.016$ ). Aq, aqueduct; BFP, blue fluorescence protein; CeA, central amygdala; ChR2, channelrhodopsin-2; IPSCs, inhibitory postsynaptic currents; IPAG, lateral periaqueductal gray; vIPAG, ventrolateral periaqueductal gray. \* $P < 0.05$ , \*\* $P < 0.01$ . All data are expressed as mean  $\pm$  SD.

and female animals were included, but no formal statistical comparisons are made to examine sex differences in the current study. These results are in line with a previous finding that female rodents are resistant to chronic restraint stress-induced thermal hyperalgesia.<sup>46</sup> Because female mice are intrinsically more variable than males, male mice were chosen for the following experiments.

To determine whether the central amygdala and ventrolateral periaqueductal gray are involved in chronic stress-related pain, *c-fos-tTA* mice, which displayed stable labeling of activated neurons by *c-Fos* promoter-driven enhanced green fluorescent protein expression,<sup>42,47</sup> were used. We found that 3-week chronic restraint stress induced massive *c-Fos* expression in the central amygdala, ventrolateral

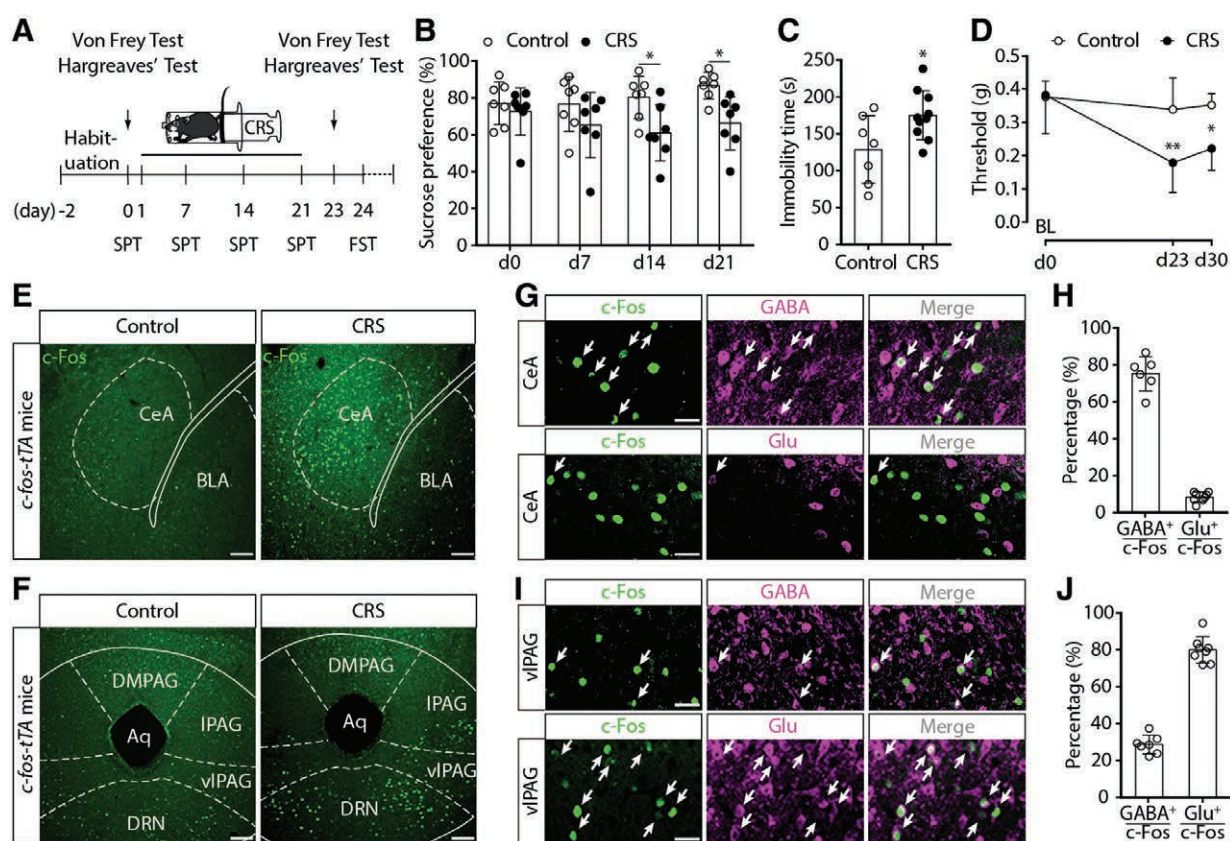


**Fig. 3.** Increased c-Fos expression in central amygdala  $\gamma$ -aminobutyric acid–mediated neurons and ventrolateral periaqueductal gray glutamatergic neurons of mice show depression-related behavior and pain sensitization. (A) Experimental design: Mice underwent a 3-week restraint stress protocol, 6 h per day; the sucrose preference test was conducted every 7 days, the mechanical and thermal withdrawal thresholds were tested pre- and postchronic restraint stress, and the forced swim test was carried out 1 day after the last Hargreave test. (B) Chronic restraint stress decreased preference for sucrose ( $n = 7$  per group; two-way repeated-measures ANOVA: time,  $F[3, 36] = 0.713$ ,  $P = 0.551$ ; chronic restraint stress,  $F[1, 12] = 11.17$ ,  $P = 0.006$ ; time  $\times$  chronic restraint stress,  $F[3, 36] = 1.209$ ,  $P = 0.32$ ; Bonferroni *post hoc* test). (C) Chronic restraint stress decreased time struggling in the forced swim test ( $n = 7$  control,  $n = 10$  chronic restraint stress, unpaired two-tailed Student's  $t$  test,  $P = 0.029$ ). (D) The Von Frey test showed that chronic restraint stress induced profound mechanical hypersensitivity ( $n = 7$  control,  $n = 9$  chronic restraint stress; two-way repeated-measures ANOVA: time,  $F[2, 28] = 9.201$ ,  $P = 0.001$ ; chronic restraint stress,  $F[1, 14] = 8.83$ ,  $P = 0.01$ ; time  $\times$  chronic restraint stress,  $F[2, 28] = 4.482$ ,  $P = 0.021$ ; Bonferroni *post hoc* test). (E) Chronic restraint stress elicited robust c-Fos expression in the central amygdala. Scale bar, 100  $\mu$ m. (F) Chronic restraint stress elicited robust c-Fos expression in the ventrolateral periaqueductal gray. Scale bar, 100  $\mu$ m. (G) Representative images of c-Fos (green, top left and bottom left),  $\gamma$ -aminobutyric acid (GABA; purple, top middle), and glutamate (purple, bottom middle) staining in the central amygdala from chronic restraint stress *c-fos-tTA* mice. Scale bar, 25  $\mu$ m. (H) Quantification of (G) shows most c-Fos<sup>+</sup> central amygdala cells expressing GABA.  $n = 6$ –8 slices (0.016 mm<sup>2</sup> imaging area per slice) from three mice per group. (I) Representative images of c-Fos (green, top left and bottom left), GABA (purple, top middle), and glutamate (purple, bottom middle) staining in the ventrolateral periaqueductal gray from chronic restraint stress *c-fos-tTA* mice. Scale bar, 25  $\mu$ m. (J) Quantification of (I) suggests that most c-Fos<sup>+</sup> ventrolateral periaqueductal gray cells displayed glutamate immunoreactivity.  $n = 7$  or 8 slices (0.016 mm<sup>2</sup> imaging area per slice) from three mice per group. Aq, aqueduct; BL, paw withdrawal threshold baseline; BLA, basolateral amygdala; CeA, central amygdala; CRS, chronic restraint stress; DMPAG, dorsomedial periaqueductal gray; FST, forced swim test; SPT, sucrose preference test. \* $P < 0.05$ . All data are expressed as mean  $\pm$  SD.

periaqueductal gray, and other stress-related brain regions (fig. 3, E and F; Supplemental Digital Content, fig. S4, <http://links.lww.com/ALN/C172>). Immunofluorescent staining showed that most of the c-Fos–positive central amygdala neurons colocalized with GABA and very few with glutamate (GABA:  $75.3\% \pm 9.3\%$ ,  $n = 127$  neurons from six slices of three mice; glutamate:  $8.5\% \pm 2.6\%$ ,  $n = 189$

neurons from eight slices of three mice; fig. 3, G and H). In contrast, the majority of c-Fos–positive ventrolateral periaqueductal gray neurons expressed glutamate ( $80.0\% \pm 7.1\%$ ,  $n = 171$  neurons from eight slices of three mice; fig. 3, I and J).

To examine the neuronal excitability in the central amygdala–ventrolateral periaqueductal gray circuit, whole

cell recordings of brain slices using electrodes filled with biocytin were performed in visualized ventrolateral periaqueductal gray–projecting central amygdala neurons from mice with ventrolateral periaqueductal gray infusion of the retrograde tracer cholera–toxin B subunit (fig. 4, A and B), and a triple labeling strategy with cholera–toxin B subunit, biocytin, and GABA antibody was used to identify the recorded central amygdala GABAergic neurons (fig. 4C). We found that the action potential firing rate of central amygdala GABAergic neurons in both 3-week chronic restraint stress and 7-day spared nerve

injury mice was statistically significantly increased (chronic restraint model: 10.4 [1.5, 19.5] spikes/s *vs.* 17.5 [4.5, 29.5] spikes/s,  $n = 20$  control and 18 chronic restraint stress cells,  $P = 0.001$ ; spared nerve injury model: 8 [0, 17] spikes/s *vs.* 12.0 [1.3, 21.8] spikes/s,  $n = 10$  sham and 9 spared nerve injury cells,  $P = 0.035$ ; fig. 4, D and E; Supplemental Digital Content, fig. S5, A and B, <http://links.lww.com/ALN/C172>). These results suggest that the neuronal activity of ventrolateral periaqueductal gray–projecting central amygdala GABAergic neurons is enhanced in chronic restraint stress mice.

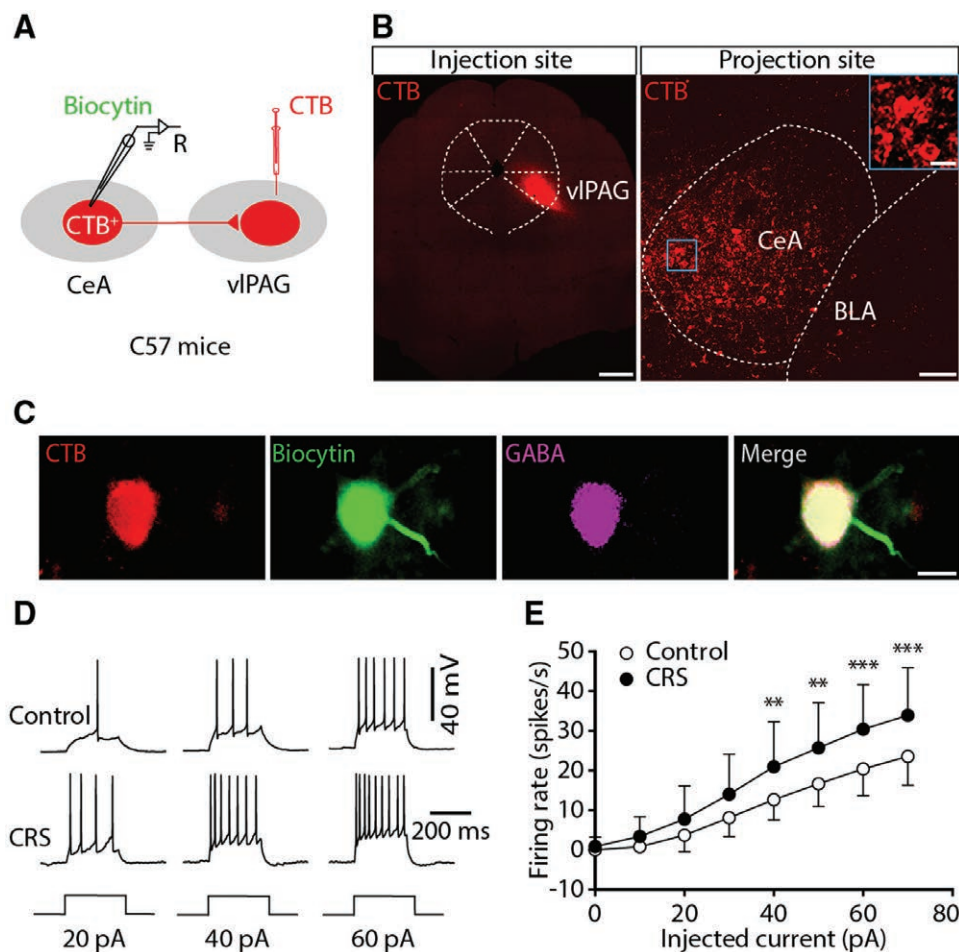


**Fig. 4.** Chronic restraint stress sensitizes ventrolateral periaqueductal gray–projecting central amygdala  $\gamma$ -aminobutyric acid–mediated (GABAergic) neurons. (A) Schematic showing whole cell recording of ventrolateral periaqueductal gray–projecting central amygdala neurons. (B) Cholera toxin B subunit injection site in ventrolateral periaqueductal gray (left, scale bar, 500  $\mu$ m). Cholera toxin B subunit–positive cells in the central amygdala (right, scale bar, 100  $\mu$ m; inset, 25  $\mu$ m). (C) Example image of a triple-labeled ventrolateral periaqueductal gray–projecting central amygdala GABAergic neuron. (D) Representative traces of voltage responses to step current injection in ventrolateral periaqueductal gray–projecting central amygdala GABAergic neurons from control and chronic restraint stress mice. (E) Summarized data showing the effect of chronic restraint stress on the firing rate of ventrolateral periaqueductal gray–projecting central amygdala GABAergic neurons.  $n = 20$  control cells;  $n = 18$  chronic restraint stress cells from three mice per group (two-way repeated-measures ANOVA: current intensity,  $F[7, 252] = 212.6$ ,  $P < 0.001$ ; chronic restraint stress,  $F[1, 36] = 10.09$ ,  $P = 0.003$ ; current intensity  $\times$  chronic restraint stress,  $F[7, 252] = 5.896$ ,  $P < 0.001$ ; Bonferroni *post hoc* test). BLA, basolateral amygdala; CeA, central amygdala; CRS, chronic restraint stress; CTB, cholera toxin B subunit; GABA,  $\gamma$ -aminobutyric acid; vIPAG, ventrolateral periaqueductal gray. \*\* $P < 0.01$ , \*\*\* $P < 0.001$ . All data are expressed as mean  $\pm$  SD.

We subsequently aimed to investigate whether inhibition of ventrolateral periaqueductal gray-projecting central amygdala GABAergic neurons could reverse pain and depressive-like behaviors. The retrogradely transported adeno-associated virus vector expressing Cre recombinase virus AAV-Retro-CMV-bG1-Cre-EGFP (Retro-Cre-GFP) was injected into the ventrolateral periaqueductal gray to deliver Cre recombinase to ventrolateral periaqueductal gray-projecting central amygdala GABAergic neurons; then we used Cre-dependent expression of the inhibitory Gi-coupled human M4 muscarinic receptor (hM4Di) in the central amygdala and intraperitoneal injection of its ligand clozapine-N-oxide selectively to inhibit ventrolateral periaqueductal gray-projecting central amygdala GABAergic neurons in C57BL/6J mice (fig. 5A). We found that hM4Di-mCherry<sup>+</sup> central amygdala neurons colocalized with GABA immunoreactivity ( $71.8\% \pm 5.5\%$ ,  $n = 4$  slices from two mice; fig. 5, B–E). Unexpectedly, clozapine-N-oxide (3mg/kg) further reduced, rather than increasing, the mechanical and thermal nociception threshold in chronic restraint stress mice (mechanical nociception:  $0.16 [0.16, 0.16]$  g *vs.*  $0.07 [0.04, 0.16]$  g,  $n = 7$  mCherry and 7 hM4Di-mCherry mice,  $P < 0.001$ ; thermal nociception:  $9.84 \pm 1.77$  s *vs.*  $6.58 \pm 3.01$  s,  $n = 8$  mCherry and 8 hM4Di-mCherry mice,  $P = 0.02$ ; fig. 5, F and G). Surprisingly, using Cre-dependent expression of the excitatory Gq-coupled human M3 muscarinic receptor (hM3Dq) in the central amygdala selectively to activate ventrolateral periaqueductal gray-projecting central amygdala GABAergic neurons, the nociception was alleviated by clozapine-N-oxide (mechanical nociception:  $0.16 \pm 0.08$  g *vs.*  $0.34 \pm 0.13$  g,  $n = 7$  mCherry and 7 hM3Dq-mCherry mice,  $P < 0.001$ ; thermal nociception:  $9.84 \pm 1.77$  s *vs.*  $21.84 \pm 1.61$  s,  $n = 8$  mCherry and 8 hM3Dq-mCherry mice,  $P < 0.001$ ; fig. 5, H and I). In addition, neither inhibition nor activation of ventrolateral periaqueductal gray-projecting central amygdala GABAergic neurons affected the depressive-like behaviors induced by chronic restraint stress (sucrose preference:  $61.1\% \pm 12.9\%$  *vs.*  $57.3\% \pm 9.0\%$  *vs.*  $62.6\% \pm 8.6\%$ ;  $n = 9$  mCherry, 8 hM3Dq-mCherry, and 8 hM4Di-mCherry mice,  $P = 0.586$ ; immobility:  $157.3 \pm 38.2$  s *vs.*  $165.6 \pm 42.6$  s *vs.*  $152.7 \pm 27.7$  s;  $n = 8$  mCherry, 8 hM3Dq-mCherry and 8 hM4Di-mCherry mice,  $P = 0.778$ ; fig. 5, J and K).

To determine the role of specific projections from the central amygdala GABAergic neurons to the ventrolateral periaqueductal gray, we infused a Cre-dependent AAV-EF1-DIO-NpHR-eYFP into the central amygdala to inhibit the activity of central amygdala GABAergic axon projections in *GAD2-Cre* mice (fig. 6, A–D). Optical inhibition in the ventrolateral periaqueductal gray had no effect on the mechanical nociception threshold in chronic restraint stress mice ( $0.16 [0.07, 0.16]$  g *vs.*  $0.16 [0.16, 0.16]$  g,  $n = 8$  eYFP and 7 NpHR-eYFP mice,  $P = 0.067$ ; fig. 6E). In contrast, optical stimulation of central amygdala GABAergic

terminals in the ventrolateral periaqueductal gray by central amygdala infusion of AAV-EF1-DIO-ChR2-mCherry increased the pain threshold in chronic restraint stress, spared nerve injury, and naïve mice (chronic restraint stress model:  $0.16 [0.16, 0.16]$  g *vs.*  $0.4 [0.4, 0.4]$  g,  $n = 8$  mCherry and 7 ChR2-mCherry mice,  $P < 0.001$ ; spared nerve injury:  $0.10 \pm 0.03$  g *vs.*  $0.40 \pm 0.07$  g,  $n = 8$  mice per group,  $P < 0.001$ ; naïve mice: mechanical nociception,  $0.44 \pm 0.04$  g *vs.*  $0.74 \pm 0.10$  g,  $n = 8$  mCherry and 8 ChR2-mCherry mice,  $P < 0.001$ ; naïve mice: thermal nociception,  $14.41 \pm 1.71$  s *vs.*  $25.32 \pm 2.38$  s,  $n = 8$  mCherry and 8 ChR2-mCherry mice,  $P < 0.001$ ; fig. 6, F–K; Supplemental Digital Content, fig. S5, C and D, and fig. S6, A–C, <http://links.lww.com/ALN/C172>). These results were consistent with the results from chemogenetic manipulations in the central amygdala GABAergic neurons and optogenetic activation of ventrolateral periaqueductal gray glutamatergic neurons ( $0.40 [0.40, 0.40]$  g *vs.*  $0.6 [0.6, 0.6]$  g,  $n = 8$  mice,  $P < 0.001$ ; fig. 6, L and M). However, neither activation nor inhibition of the central amygdala-ventrolateral periaqueductal gray GABAergic pathway induced depressive-like behaviors in naïve mice (sucrose preference:  $74.4\% \pm 18.9\%$  *vs.*  $80.2\% \pm 12.3\%$  *vs.*  $78.7\% \pm 9.9\%$ ,  $n = 8$  mice per group,  $P = 0.7$ ; tail suspension immobility time:  $93.2 \pm 22.7$  s *vs.*  $105.9 \pm 24.4$  s *vs.*  $93.8 \pm 18.2$  s,  $n = 8$  mice per group,  $P = 0.439$ ; Supplemental Digital Content, fig. S6, A, D, and E, <http://links.lww.com/ALN/C172>). These results suggest that an activated central amygdala-ventrolateral periaqueductal gray GABAergic pathway exerts an analgesic effect.

### Disinhibition of the Ventrolateral Periaqueductal Gray Local Circuit in Mice Exposed to Chronic Restraint Stress

If the ventrolateral periaqueductal gray local microcircuit is innervated by central amygdala GABAergic inputs, the increase of the inputs under depression conditions should cause disinhibitory effects. To determine the neuronal excitability of the ventrolateral periaqueductal gray neurons, we performed whole cell recordings on the visualized ventrolateral periaqueductal gray GABAergic and glutamatergic neurons by crossing *GAD2-Cre* or *CaMKII-Cre* mice with Rosa26-LSL-tdTomato mice (Ai9 line) to produce transgenic mice with red tdTomato-expressing GABA (*GAD2-tdTOM*) or glutamate (*CaMKII-tdTOM*) neurons (fig. 7A).<sup>48,49</sup> Indeed, we found a decrease in the spike number in ventrolateral periaqueductal gray GABAergic neurons from both chronic restraint stress and spared nerve injury mice compared with control mice (chronic restraint stress model:  $34.7 \pm 19.2$  spikes/s *vs.*  $23.3 \pm 13.2$  spikes/s,  $n = 19$  control and 15 chronic restraint stress cells from three mice per group,  $P < 0.001$ ; spared nerve injury model:  $40.2 \pm 18.4$  spikes/s *vs.*  $23.5 \pm 10.0$  spikes/s,  $n = 13$  cells from three mice per group,  $P < 0.001$ ; fig. 7, B and C; Supplemental Digital Content, fig. S5, E and F, <http://links.lww.com/ALN/C172>). In addition, chronic restraint stress increased the frequency of miniature inhibitory postsynaptic currents in ventrolateral periaqueductal gray GABAergic

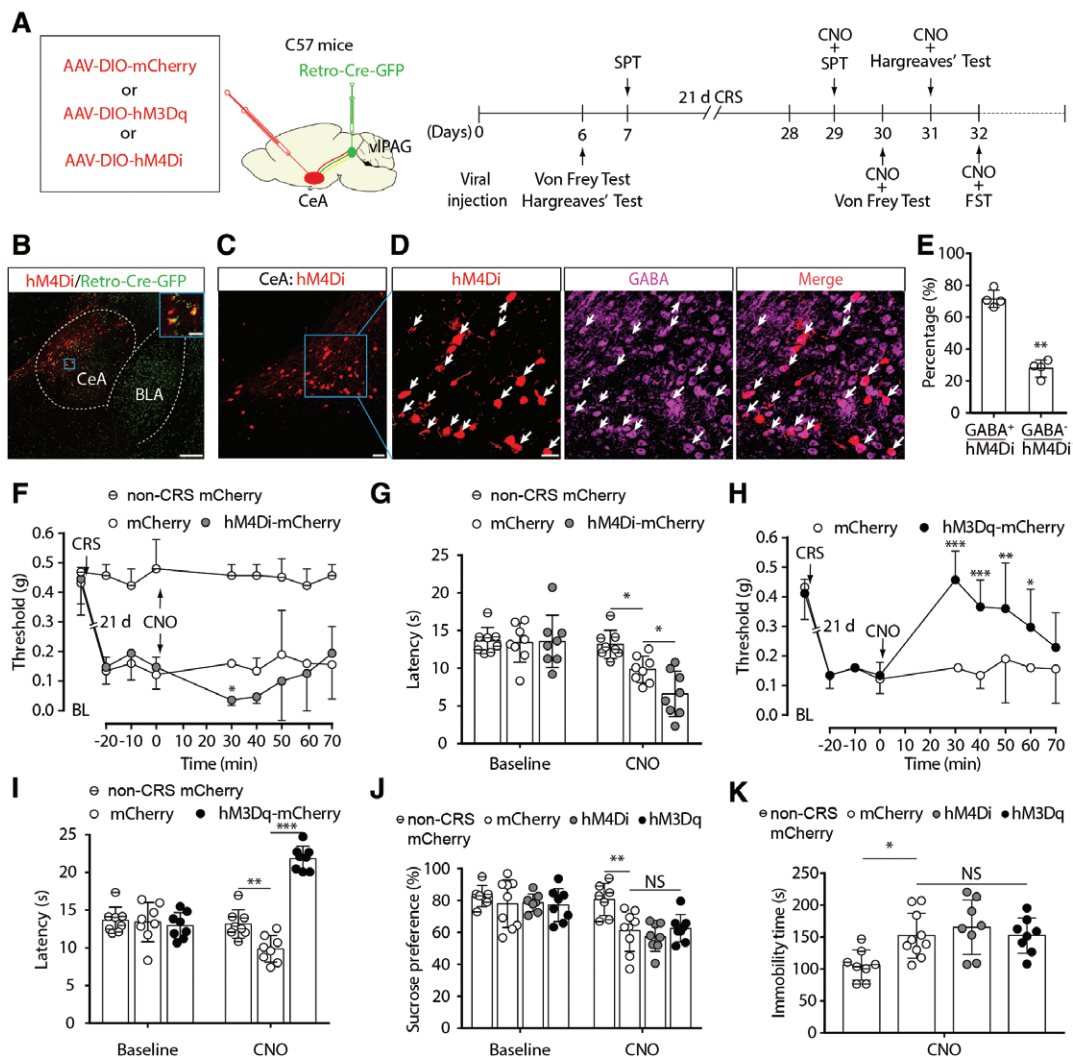


**Fig. 5.** The ventrolateral periaqueductal gray-projecting central amygdala  $\gamma$ -aminobutyric acid-mediated neurons bidirectionally modulated nociception. (A) Schematic showing the injection of AAV-retro-Cre into the ventrolateral periaqueductal gray and of chemogenetic virus into the central amygdala in a wild-type mouse (left). The experimental timeline (right) for (F–K). (B) Expression of hM4Di in ventrolateral periaqueductal gray-projecting central amygdala neurons in C57BL/6 mice. Scale bar, 200  $\mu$ m; inset, 25  $\mu$ m. (C) hM4Di-mCherry expression in the central amygdala. Scale bar, 50  $\mu$ m. (D) Panels show a close-up view of the blue box shown in (C) and overlap between hM4Di-mCherry<sup>+</sup> and  $\gamma$ -aminobutyric acid (GABA)<sup>+</sup> neurons. Scale bar, 20  $\mu$ m. (E) Quantification of GABA<sup>+</sup> neurons in ventrolateral periaqueductal gray-projecting central amygdala neurons ( $n = 4$  slices from two mice, two-tailed paired Student's  $t$  test,  $P = 0.004$ ). (F) The Von Frey test showed that clozapine-N-oxide induced further mechanical hypersensitivity in the hM4Di group mice ( $n = 7$  per group; two-way repeated-measures ANOVA: time,  $F_{[8, 144]} = 13.48$ ,  $P < 0.001$ ; clozapine-N-oxide,  $F_{[2, 18]} = 56.87$ ,  $P < 0.001$ ; time  $\times$  clozapine-N-oxide,  $F_{[16, 144]} = 3.962$ ,  $P < 0.001$ ; Bonferroni *post hoc* test). (G) Clozapine-N-oxide intensified chronic restraint stress induced-thermal hypersensitivity in the hM4Di group mice ( $n = 8$  per group; two-way repeated-measures ANOVA: time,  $F_{[1, 21]} = 40.33$ ,  $P < 0.001$ ; clozapine-N-oxide,  $F_{[2, 21]} = 5.219$ ,  $P = 0.015$ ; time  $\times$  clozapine-N-oxide,  $F_{[2, 21]} = 10.54$ ,  $P = 0.001$ ; Bonferroni *post hoc* test). (H) The Von Frey test showed that clozapine-N-oxide reversed the mechanical hyperalgesia of hM3Dq group mice ( $n = 7$  per group; two-way repeated-measures: time,  $F_{[8, 96]} = 23.14$ ,  $P < 0.001$ ; clozapine-N-oxide,  $F_{[1, 12]} = 19.97$ ,  $P = 0.001$ ; time  $\times$  clozapine-N-oxide,  $F_{[8, 96]} = 8.522$ ,  $P < 0.001$ ; Bonferroni *post hoc* test). (I) Clozapine-N-oxide reversed chronic restraint stress induced-thermal hypersensitivity in hM3Dq group mice ( $n = 8$  per group; two-way repeated-measures ANOVA: time,  $F_{[1, 21]} = 10.47$ ,  $P = 0.004$ ; clozapine-N-oxide,  $F_{[2, 21]} = 32.36$ ,  $P < 0.001$ ; time  $\times$  clozapine-N-oxide,  $F_{[2, 21]} = 55.62$ ,  $P < 0.001$ ; Bonferroni *post hoc* test). (J) Clozapine-N-oxide has no effect on chronic restraint stress induced-sucrose preference decrease ( $n = 7$  nonchronic restraint stress mCherry, 9 mCherry, 8 hM4Di, 8 hM3Dq; two-way repeated-measures ANOVA: time,  $F_{[1, 28]} = 46.19$ ,  $P < 0.001$ ; clozapine-N-oxide,  $F_{[3, 28]} = 3.914$ ,  $P = 0.019$ ; time  $\times$  clozapine-N-oxide,  $F_{[3, 28]} = 3.833$ ,  $P = 0.02$ ; Bonferroni *post hoc* test). (K) Clozapine-N-oxide has no effect on chronic restraint stress induced-decreased time struggling in the forced swim test ( $n = 7$  nonchronic restraint stress mCherry, 9 mCherry, 8 hM4Di, 8 hM3Dq; ordinary one-way ANOVA: clozapine-N-oxide,  $F_{[3, 30]} = 4.965$ ,  $P = 0.007$ ; Bonferroni *post hoc* test). BLA, basolateral amygdala; CeA, central amygdala; CNO, clozapine-N-oxide; CRS, chronic restraint stress; FST, forced swim test; hM3Dq, Gq-coupled human M3 muscarinic receptor; hM4Di, Gi-coupled human M4 muscarinic receptor; NS, no significant difference; SPT, sucrose preference test. \* $P < 0.05$ , \*\* $P < 0.01$ , \*\*\* $P < 0.001$ . All data are expressed as mean  $\pm$  SD.

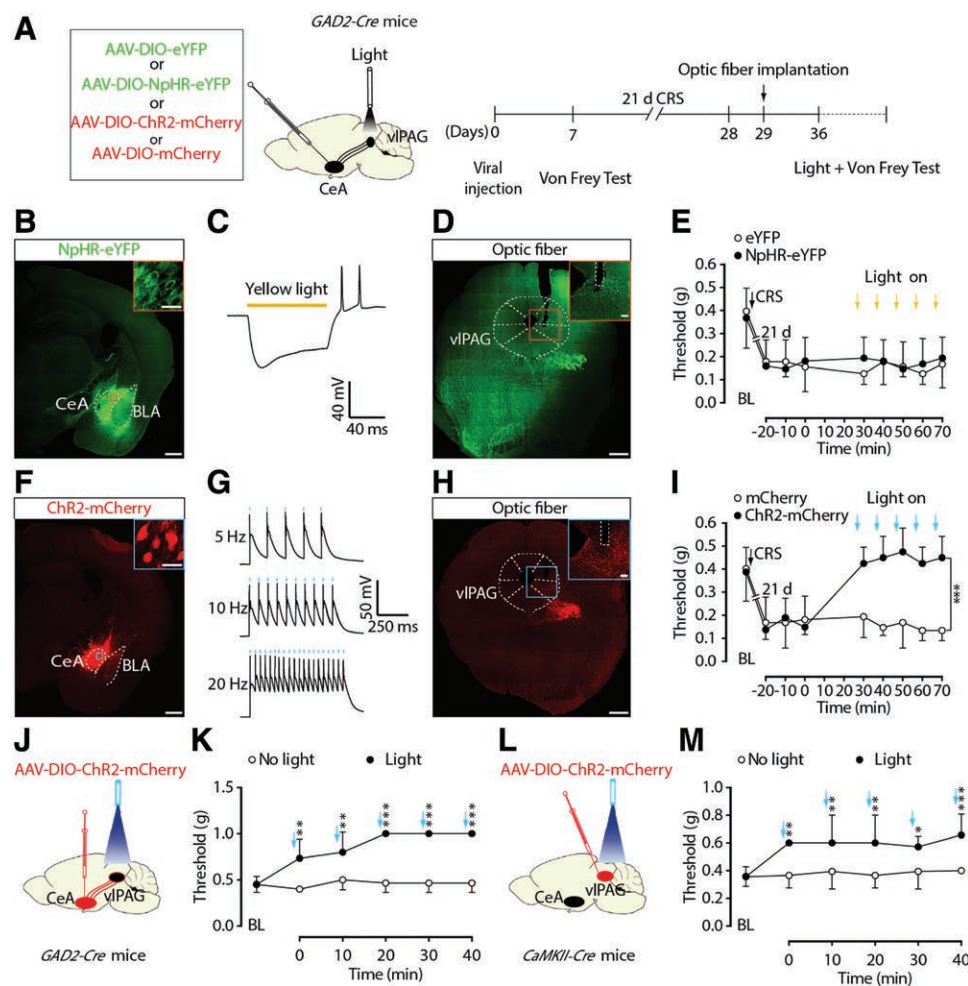


**Fig. 6.** Activation of central amygdala  $\gamma$ -aminobutyric acid–mediated (GABAergic) terminals in the ventrolateral periaqueductal gray relieves pain sensitization. (A) Schematic of viral injections and optic fiber implantations in ventrolateral periaqueductal gray for optogenetic manipulations and experimental timeline for (E) and (I). (B) Expression of NpHR in the central amygdala. Scale bar, 500  $\mu$ m; inset, 25  $\mu$ m. (C) Voltage response of NpHR-positive neurons in the central amygdala after photostimulation (100 ms, yellow bar). (D) Representative image of NpHR-positive fibers in ventrolateral periaqueductal gray implanted with an optical fiber (white dashed line indicates fiber track). Scale bar, 500  $\mu$ m; inset, 100  $\mu$ m. (E) Inhibition of central amygdala GABAergic terminals in ventrolateral periaqueductal gray caused no change in mechanical thresholds ( $n = 8$  eYFP,  $n = 7$  NpHR; two-way repeated-measures ANOVA: time,  $F[8, 104] = 14.53$ ,  $P < 0.001$ ; light,  $F[1, 13] = 0.147$ ,  $P = 0.708$ ; time  $\times$  light,  $F[8, 104] = 0.791$ ,  $P = 0.611$ ; Bonferroni *post hoc* test). (F) Expression of ChR2 in the central amygdala. Scale bar, 500  $\mu$ m; inset, 25  $\mu$ m. (G) Action potentials induced by photostimulation (473 nm, 10 ms, blue bars) in central amygdala GABAergic neurons. (H) Representative image of ChR2-positive fibers in ventrolateral periaqueductal gray implanted with an optical fiber (white dashed line indicates fiber track). Scale bar, 500  $\mu$ m; inset, 100  $\mu$ m. (I) Activation of central amygdala GABAergic terminals in ventrolateral periaqueductal gray caused strong hyposensitivity ( $n = 8$  mCherry,  $n = 7$  ChR2; two-way repeated-measures ANOVA: time,  $F[8, 104] = 17.6$ ,  $P < 0.001$ ; light,  $F[1, 13] = 85.64$ ,  $P < 0.001$ ; time  $\times$  light,  $F[8, 104] = 16.47$ ,  $P < 0.001$ ; Bonferroni *post hoc* test). (J) Schematic showing the stimulation of the ChR2-expressing terminals from the central amygdala in the ventrolateral periaqueductal gray of *GAD2-Cre* mice. (K) Light activation of ChR2-expressing terminals from the central amygdala in the ventrolateral periaqueductal gray induced analgesia ( $n = 6$ , two-way repeated-measures ANOVA: time,  $F[5, 25] = 23.63$ ,  $P < 0.001$ ; light,  $F[1, 5] = 423.5$ ,  $P < 0.001$ ; time  $\times$  light,  $F[5, 25] = 7.835$ ,  $P < 0.001$ ; Bonferroni *post hoc* test). (L) Schematic showing the stimulation of the ChR2-expressing ventrolateral periaqueductal gray glutamatergic neurons of *CaMKII-Cre* mice. (M) Light activation of ChR2-expressing ventrolateral periaqueductal gray glutamatergic neurons induced analgesia ( $n = 7$ , two-way repeated-measures ANOVA: time,  $F[5, 30] = 2.505$ ,  $P = 0.052$ ; light,  $F[1, 6] = 38.8$ ,  $P = 0.001$ ; time  $\times$  light,  $F[5, 30] = 2.988$ ,  $P = 0.026$ ; Bonferroni *post hoc* test). BLA, basolateral amygdala; CeA, central amygdala; ChR2, channelrhodopsin-2; CRS, chronic restraint stress; eYFP, enhanced yellow fluorescent protein; NpHR, natronomonas pharaonis halorhodopsin; vPAG, ventrolateral periaqueductal gray. \* $P < 0.05$ , \*\* $P < 0.01$ , \*\*\* $P < 0.001$ . All data are expressed as mean  $\pm$  SD.

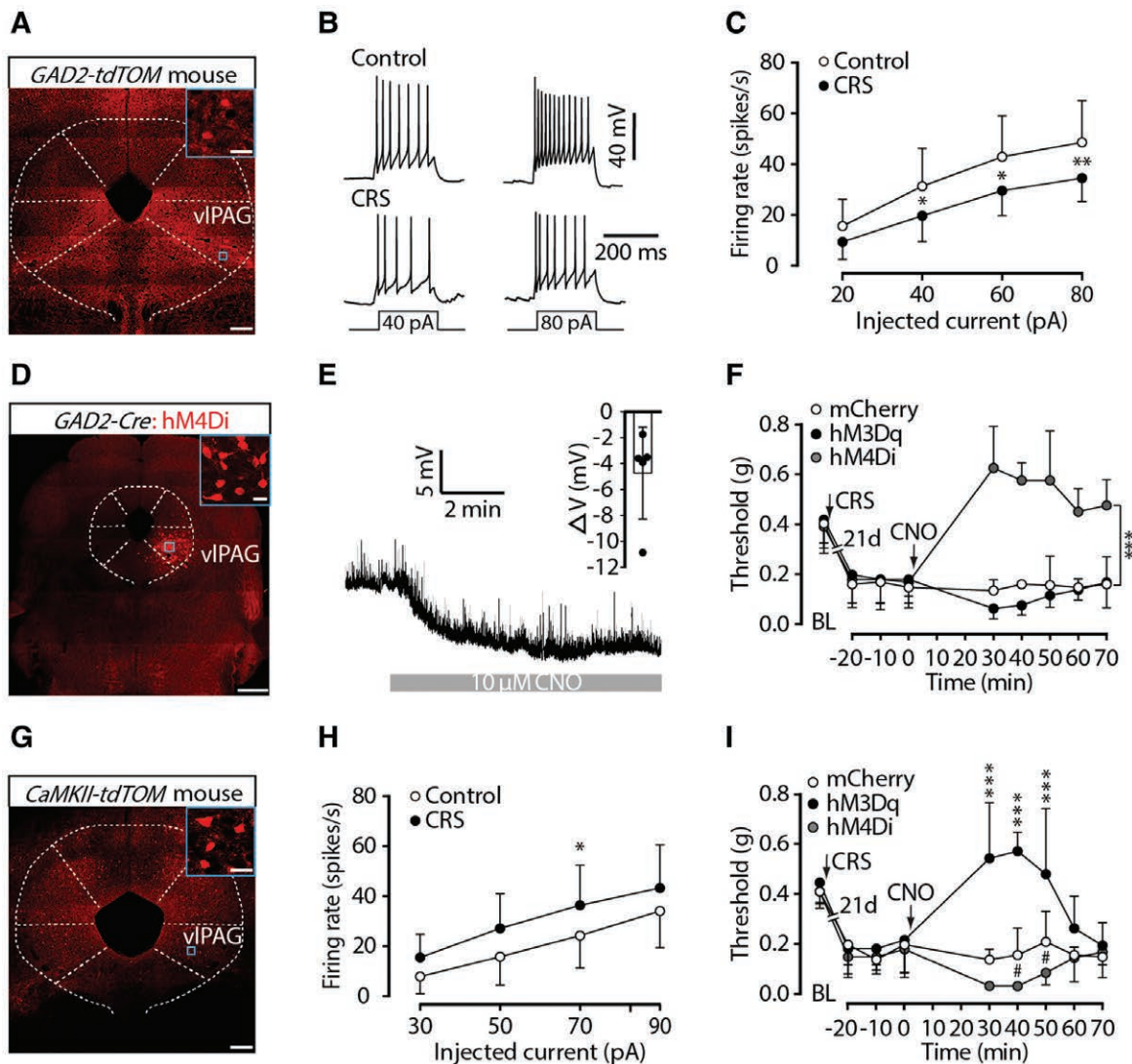


**Fig. 7.** The ventrolateral periaqueductal gray  $\gamma$ -aminobutyric acid-mediated (GABAergic) and glutamatergic neurons exert bidirectional modulation on nociception. (A) An example image of the ventrolateral periaqueductal gray from a *GAD2-tdTOM* mouse. Scale bar, 200  $\mu$ m; inset, 25  $\mu$ m. (B) Representative traces of voltage responses to step current injection in ventrolateral periaqueductal gray GABAergic neurons. (C) The effect of chronic restraint stress on the firing rate of ventrolateral periaqueductal gray GABAergic neurons ( $n = 19$  control cells,  $n = 15$  chronic restraint stress cells from three mice; two-way repeated-measures ANOVA: current intensity,  $F[3, 96] = 200.9$ ,  $P < 0.001$ ; chronic restraint stress,  $F[1, 32] = 7.87$ ,  $P = 0.009$ ; current intensity  $\times$  chronic restraint stress,  $F[3, 96] = 3.806$ ,  $P = 0.013$ ; Bonferroni *post hoc* test). (D) Expression of hM4Di in the ventrolateral periaqueductal gray of a *GAD2-Cre* mouse. Scale bar, 500  $\mu$ m; inset, 25  $\mu$ m. (E) Representative trace of clozapine-N-oxide-induced hyperpolarization of hM4Di<sup>+</sup> ventrolateral periaqueductal gray GABAergic neurons and the quantitation of resting membrane potentials ( $n = 5$  cells, two-tailed paired Student's *t* test,  $t[4] = 2.99$ ,  $P = 0.04$ ). (F) The Von Frey test showed that clozapine-N-oxide caused strong mechanical hyposensitivity in hM4Di group mice and mechanical hypersensitivity in hM3Dq group mice ( $n = 7$  mCherry,  $n = 8$  hM3Dq,  $n = 8$  hM4Di; two-way repeated-measures ANOVA: time,  $F[8, 160] = 16.78$ ,  $P < 0.001$ ; clozapine-N-oxide,  $F[2, 20] = 99.18$ ,  $P < 0.001$ ; time  $\times$  clozapine-N-oxide,  $F[16, 160] = 18.71$ ,  $P < 0.001$ , Bonferroni *post hoc* test). (G) An example image of ventrolateral periaqueductal gray from a *CaMKII-tdTOM* mouse. Scale bar, 200  $\mu$ m; inset, 25  $\mu$ m. (H) The effect of chronic restraint stress on the firing rate of ventrolateral periaqueductal gray glutamatergic neurons ( $n = 14$  control cells,  $n = 31$  chronic restraint stress cells from three mice; two-way repeated-measures ANOVA: current intensity,  $F[3, 129] = 164.3$ ,  $P < 0.001$ ; chronic restraint stress,  $F[1, 43] = 5.543$ ,  $P = 0.023$ ; current intensity  $\times$  chronic restraint stress,  $F[3, 129] = 1.302$ ,  $P = 0.277$ ; Bonferroni *post hoc* test). (I) The Von Frey test showed that clozapine-N-oxide caused strong mechanical hyposensitivity in the hM3Dq group and mechanical hypersensitivity in the hM4Di group mice ( $n = 7$  mCherry,  $n = 8$  hM3Dq,  $n = 8$  hM4Di; two-way repeated-measures ANOVA: time,  $F[8, 160] = 17.54$ ,  $P < 0.001$ ; clozapine-N-oxide,  $F[2, 20] = 28.43$ ,  $P < 0.001$ ; time  $\times$  clozapine-N-oxide,  $F[16, 160] = 11.62$ ,  $P < 0.001$ , Bonferroni *post hoc* test). BL, paw withdrawal threshold baseline; CNO, clozapine-N-oxide; CRS, chronic restraint stress; hM3Dq, Gq-coupled human M3 muscarinic receptor; hM4Di, Gi-coupled human M4 muscarinic receptor; vIPAG, ventrolateral periaqueductal gray. \* $P < 0.05$ , \*\* $P < 0.01$ , \*\*\* $P < 0.001$ , # $P < 0.05$ . All data are expressed as mean  $\pm$  SD.

neurons ( $1.0 \pm 0.6$  vs.  $2.5 \pm 1.0$ ;  $n = 10$  cells from three mice per group,  $P = 0.001$ ; Supplemental Digital Content, fig. S7, A–C, <http://links.lww.com/ALN/C172>). Chemogenetic activation of ventrolateral periaqueductal gray GABAergic neurons further decreased the mechanical nociception threshold in chronic restraint stress mice, while inhibition of these neurons statistically significantly increased the mechanical nociception threshold (activation:  $0.16 [0.16, 0.16]$  g vs.  $0.07 [0.07, 0.16]$  g,  $n = 7$  control and 8 hM3Dq-mCherry mice,  $P = 0.001$ ; inhibition:  $0.16 [0.16, 0.16]$  g vs.  $0.40 [0.40, 0.60]$  g,  $n = 7$  control and 8 hM4Di-mCherry mice,  $P < 0.001$ ; fig. 7, D–F). In contrast, the excitability of the ventrolateral periaqueductal gray glutamatergic neurons was increased in both chronic restraint stress and spared nerve injury mice (chronic restraint stress model:  $20.5 \pm 15.5$  spikes/s vs.  $30.6 \pm 18.1$  spikes/s,  $n = 14$  control and 31 chronic restraint stress cells from three mice per group,  $P < 0.001$ ; spared nerve injury model:  $12.7 [0.3, 20.0]$  spikes/s vs.  $19.4 \pm 15.0$  spikes/s,  $n = 11$  sham and 10 spared nerve injury cells from three mice per group,  $P = 0.028$ ; fig. 7, G and H; Supplemental Digital Content, fig. S5, E and G, <http://links.lww.com/ALN/C172>). Moreover, chronic restraint stress decreased the amplitude of miniature inhibitory postsynaptic currents in ventrolateral periaqueductal gray glutamatergic neurons ( $32.7 \pm 12.6$  pA vs.  $23.3 \pm 9.4$  pA;  $n = 17$  control and 20 chronic restraint stress cells from three mice per group;  $P = 0.014$ ; Supplemental Digital Content, fig. S7, D–F, <http://links.lww.com/ALN/C172>). Chemogenetic inhibition of ventrolateral periaqueductal gray glutamatergic neurons caused further mechanical hyperalgesia in chronic restraint stress mice, whereas activation of these neurons alleviated it (activation:  $0.16 [0.09, 0.16]$  g vs.  $0.40 [0.16, 0.60]$  g,  $n = 8$  control and 7 hM3Dq-mCherry mice,  $P < 0.001$ ; inhibition:  $0.16 [0.09, 0.16]$  g vs.  $0.07 [0.04, 0.16]$  g,  $n = 8$  control and 8 hM4Di-mCherry mice,  $P < 0.001$ ; fig. 7I).

To confirm the function of the central amygdala–ventrolateral periaqueductal gray circuit in nociception induced by chronic restraint stress, we injected AAV-CMV-bGlu-Cre-EGFP into the central amygdala and chemogenetic virus into the ipsilateral ventrolateral periaqueductal gray (fig. 8, A and B). Given the strong inhibitory microcircuit within this mixed population of ventrolateral periaqueductal gray GABAergic and glutamatergic neurons, chemogenetic inhibition of these neurons may produce mechanical hyperalgesia. As expected, we found that clozapine-N-oxide had no effect on the nociception of hM3Dq-expressing mice, whereas it reduced the mechanical nociception threshold in hM4Di-expressing mice (inhibition:  $0.40 [0.40, 0.40]$  g vs.  $0.07 [0.07, 0.16]$  g,  $n = 7$  control and 8 hM4Di-mCherry mice,  $P < 0.001$ ; activation:  $0.40 [0.40, 0.40]$  g vs.  $0.40 [0.40, 0.40]$  g,  $n = 7$  control and 8 hM3Dq-mCherry mice,  $P = 0.96$ ; fig. 8, C and D). Together, these results suggest that the central amygdala–ventrolateral periaqueductal gray circuit is, at least in part, an endogenous analgesic circuit under depression conditions (fig. 9).

## Discussion

This study defines a central amygdala–ventrolateral periaqueductal gray circuit, which is involved in nociception under chronic restraint stress conditions in a mouse model. Central to this process is a circuit mechanism involving the enhanced inhibition of central amygdala GABAergic neurons projecting to ventrolateral periaqueductal gray GABAergic neurons, which disinhibits local glutamatergic neurons. It is important to note that reducing the activity of this circuit fails to rescue the nociception induced by chronic restraint stress, whereas further activating this circuit alleviates nociception. These findings suggest that the increased activity of this circuit may play a role in coping with nociception in depressive states.

A body of evidence from human brain imaging studies has shown an altered functional connectivity between the amygdala and periaqueductal gray in a pain setting. For example, patients with fibromyalgia were found to have increased periaqueductal gray connectivity with the amygdala,<sup>50</sup> while pain-related fear led to a decrease in amygdala–periaqueductal gray functional connectivity in chronic low back pain patients.<sup>51</sup> In addition, higher pain led to an increased functional connectivity between the periaqueductal gray and the amygdala in healthy men.<sup>13</sup> Interestingly, acupuncture could increase amygdala connectivity with the periaqueductal gray and insula.<sup>52</sup> These studies suggest the involvement of the amygdala–periaqueductal gray pathway in human pain. In the current study, we revealed increased activity of the central amygdala–ventrolateral periaqueductal gray pathway in mice manifesting pain symptoms under depression conditions; further activation of this pathway reversed rather than intensifying the pain symptom. Therefore, the increased activity of this circuitry is likely a compensatory effect attempting to counteract the pain symptom caused by chronic stress. These results from mice are consistent with previous findings from humans that there is increased functional connectivity between the amygdala and periaqueductal gray in the pain setting and that the functional connectivity is decreased by acupuncture.

The relationship between restraint stress and pain sensitivity has been shown to be quite complex. It varies from acute to chronic restraint stress,<sup>45,46</sup> and from males to females.<sup>53</sup> Generally, acute restraint stress decreases and chronic restraint stress increases pain sensitivity.<sup>45,46</sup> However, there seems to be a gender-specific nociceptive response in both acute and chronic restraint stress. It has been reported that acute restraint stress does not alter formalin-induced mechanical hypersensitivity in female mice,<sup>54</sup> while repeated restraint stress decreases tail-flick latency only in male rats.<sup>46</sup> In the current study, we first examined the nociception to a mechanical stimulus in male mice after 3-week restraint stress based on the assumption that females are intrinsically more variable than males, and found that male mice showed increased mechanical and thermal nociception, which is in line with previous studies.<sup>45</sup> Females are more pain-sensitive because of the higher basal level of

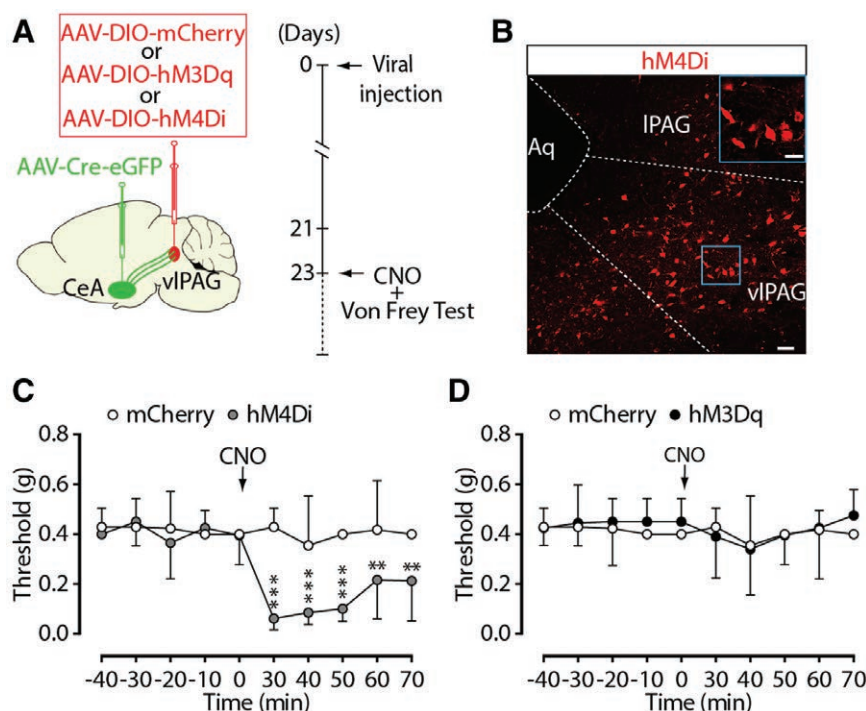


**Fig. 8.** The ventrolateral periaqueductal gray neurons innervated by central amygdala bidirectionally modulate nociception. (A) Schematic showing the injection of AAV-Cre-eGFP into the central amygdala and of chemogenetic virus into the ventrolateral periaqueductal gray in a wild-type mouse (*left*). The experimental timeline (*right*). (B) hM4Di-mCherry expression in the ventrolateral periaqueductal gray. Scale bar, 50  $\mu$ m; inset, 25  $\mu$ m. (C) Clozapine-N-oxide caused mechanical hypersensitivity of the hM4Di group mice ( $n = 7$  mCherry,  $n = 8$  hM4Di; two-way repeated-measures ANOVA: time,  $F_{9,117} = 10.85$ ,  $P < 0.001$ ; clozapine-N-oxide,  $F_{1,13} = 24.51$ ,  $P < 0.001$ ; time  $\times$  clozapine-N-oxide,  $F_{9,117} = 8.595$ ,  $P < 0.001$ , Bonferroni *post hoc* test). (D) Clozapine-N-oxide had no effect on the mechanical threshold of the hM3Dq group mice ( $n = 7$  mCherry,  $n = 8$  hM3Dq; two-way repeated-measures ANOVA: time,  $F_{9,117} = 1.192$ ,  $P = 0.306$ ; clozapine-N-oxide,  $F_{1,13} = 0.278$ ,  $P = 0.607$ ; time  $\times$  clozapine-N-oxide,  $F_{9,117} = 0.473$ ,  $P = 0.89$ , Bonferroni *post hoc* test). Aq, aqueduct; CeA, central amygdala; CNO, clozapine-N-oxide; hM3Dq, Gq-coupled human M3 muscarinic receptor; hM4Di, Gi-coupled human M4 muscarinic receptor; IPAG, lateral periaqueductal gray; vIPAG, ventrolateral periaqueductal gray. \*\* $P < 0.01$ , \*\*\* $P < 0.001$ . All data are expressed as mean  $\pm$  SD.

corticosterone,<sup>55</sup> greater variability in hormone responses to stress,<sup>56</sup> and less efficient endogenous pain inhibitory capacity compared with males.<sup>57</sup> The activity of hypothalamic pituitary adrenal axis and level of extracellular signal regulated kinase 2 within the central amygdala may also account for the sex-based differences of formalin-induced pain-like behavior after acute restraint stress.<sup>54</sup> We found the chronic restraint stress induced mechanical nociception in female mice, but not thermal nociception. These results are consistent with the abovementioned studies, which found that female rodents have in-built resistance to restraint stress-induced nociception alteration.<sup>46,54</sup> Therefore, many factors could contribute to sex differences in the chronic restraint stress model; the mechanism needs further investigation.

In the current study, ketamine was used to produce rapid sedative/analgesic effects, and to avoid the death of animals during the viral injection surgery by preserving the protective airway reflexes.<sup>58</sup> However, ketamine at subanesthetic doses probably affected pain and emotion in humans.<sup>59–61</sup> Notably, in mice, it has been shown that ketamine-induced

antidepressant effects last up to 7 days,<sup>62,63</sup> while the mechanical and cold hypersensitivity is not affected when neuropathic pain has been established.<sup>64</sup> In the current study, behavioral tests were conducted at least 3 weeks after a single ketamine injection. Therefore, ketamine may have no long-lasting effect on pain in a mouse model of depression-like behavior.

Traditional analgesics seem to have limited effects on pain with depression.<sup>1</sup> Understanding why the treatment for depression patients with pain is far from satisfactory represents a major challenge. Currently, serotonin and norepinephrine reuptake inhibitors and tricyclic antidepressants are typical antidepressants for the treatment of depression with a variety of chronic pain conditions. However, limited data suggest that serotonin and norepinephrine reuptake inhibitors or tricyclic antidepressants may be promising for the treatment of pain-related disorders, including depression in patients with multiple somatic complaints, which is presumably due to the role of serotonin in both inhibiting and enhancing pain *via* descending pathways.<sup>65</sup> Notably, the exact targets for these drugs are unclear. For their analgesic

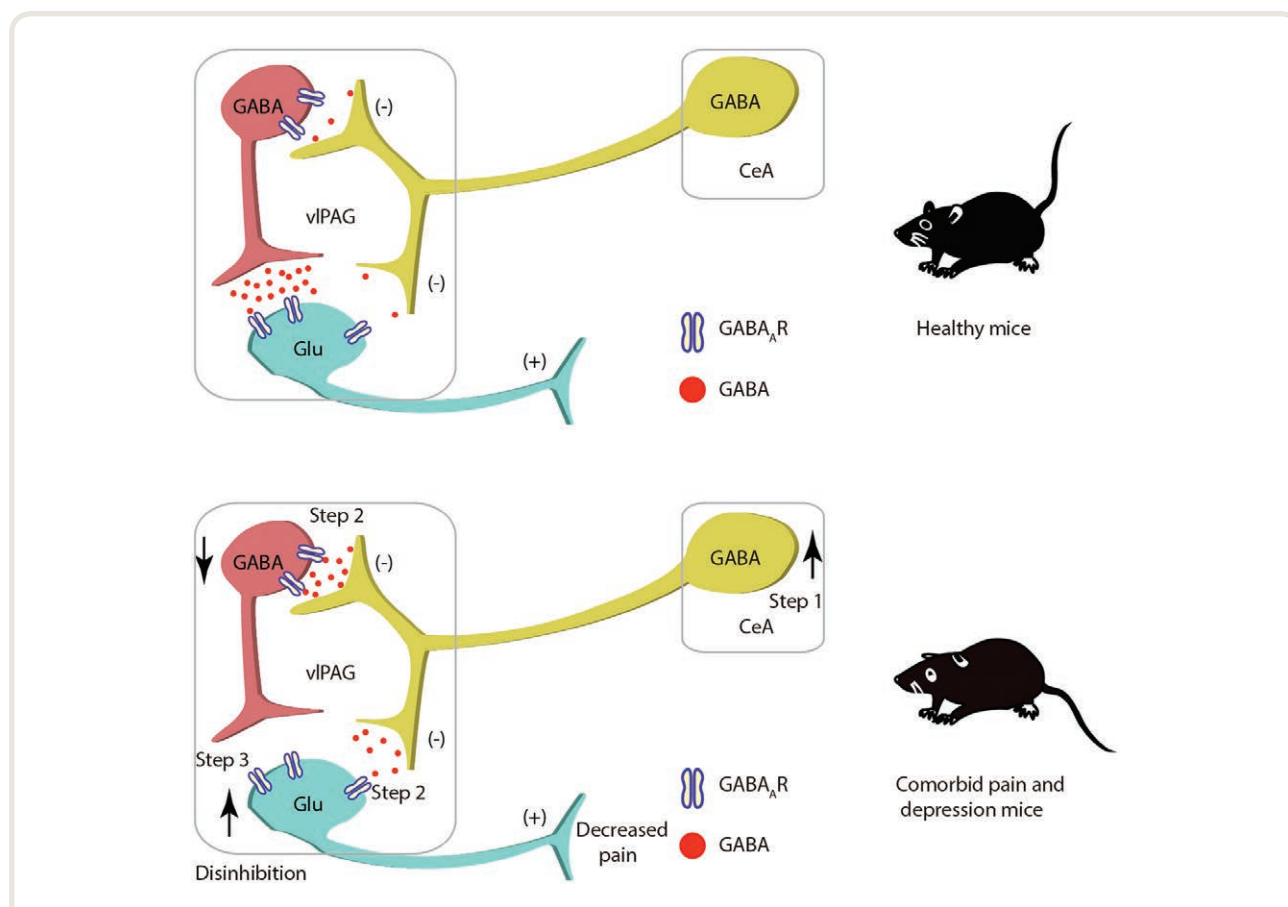


**Fig. 9.** The neural circuit mechanisms underlying nociception in depression. In the depression state, a decreased inhibitory process occurs within the ventrolateral periaqueductal gray, which involves increased central amygdala  $\gamma$ -aminobutyric acid-mediated (GABAergic) inputs (*brown*) that mediate disinhibition of the ventrolateral periaqueductal gray glutamatergic neurons (*blue*). The alterations lead to low excitation of the ventrolateral periaqueductal gray GABAergic neurons. As a result, the inhibitory ventrolateral periaqueductal gray GABAergic outputs (*purple*) to the ventrolateral periaqueductal gray glutamatergic neurons are decreased, and this insufficient alteration presumably causes nociception. CeA, central amygdala; GABA,  $\gamma$ -aminobutyric acid; GABA<sub>A</sub>R,  $\gamma$ -aminobutyric acid type A receptor; Glu, glutamate; vIPAG, ventrolateral periaqueductal gray.

effects, one possible mechanism is the activation of the descending modulatory pathway from the rostral ventromedial medulla and periaqueductal gray to the dorsal horn neurons. The current findings suggest that the neuroanatomical and molecular substrates that underlie pain in depression may differ from the known substrates that underlie pain, and the descending pain modulatory pathway is probably required for pain in depression.

The advantage of studying the neural circuit mechanism of a disorder seems to reveal the convergent point of drug actions and pathologic behavioral consequences. Unfortunately, such a mechanism for pain in depression remains unknown. Herein, we aimed to investigate a novel neuronal circuitry mechanism underlying nociception in a mouse model of depression. Based on our current findings, we would like to propose a hypothesis for the neural circuit mechanism of pain in depression, for which depression could cause enhanced inhibition of the central amygdala GABAergic inputs onto ventrolateral

periaqueductal gray GABAergic neurons, and thus reduced inhibitory outputs to ventrolateral periaqueductal gray glutamatergic neurons, leading to pain symptoms. It is striking that alterations of this circuit under depression conditions are responsible for the alleviation, but not the development, of depression-induced nociception. These findings suggest that the central amygdala–ventrolateral periaqueductal projection is a new circuitry for analgesia but not nociception in depression states. A possible reason is that chronic restraint stress activates a series of emotion-related brain nuclei, which involves both descending pain facilitation and inhibition pathways. The decreased nociception threshold is likely the net effect of these convergent pathways. Indeed, in a recent study, François *et al.* reported activated rostral ventromedial medulla/spinal/primary circuit was recruited to mediate chronic restraint stress-induced mechanical nociception in mice, and the rostral ventromedial medulla was widely regulated by emotion-related brain nuclei such as the parabrachial nucleus,<sup>45</sup> which

has been demonstrated to be activated by chronic restraint stress in our study. Thus, the insufficient compensatory actions of the central amygdala–ventrolateral periaqueductal gray circuit are not enough to block chronic stress–induced pain symptoms.

The central amygdala–containing limbic forebrain is the crucial relay to carry emotional signals to pain centers, including the ventrolateral periaqueductal gray, to exert the emotional modulation of pain.<sup>31</sup> Such projection allows the ventrolateral periaqueductal gray, which receives emotional information from the central amygdala–GABA systems, to generate pain inhibition or facilitation by linking to distinct circuits.<sup>32,66</sup> The serial organization of ventrolateral periaqueductal gray microcircuits that we dissected shows that both central amygdala GABAergic neurons and local ventrolateral periaqueductal gray GABAergic neurons project onto ventrolateral periaqueductal gray glutamatergic neurons to exert inhibitory effects. Thus, under depression conditions, the balance of excitation of ventrolateral periaqueductal gray glutamatergic neurons was altered by disinhibition through direct enhancement of presynaptic central amygdala GABAergic inputs by the reduction of local ventrolateral periaqueductal gray GABAergic neuronal function. Overall, it is likely that these regulations of both ventrolateral periaqueductal gray GABAergic and glutamatergic neurons are concurrent in depression, largely occurring through a presynaptic central amygdala GABA mechanism.

Previous work showed that the synaptic activity and spike output of ventrolateral periaqueductal gray glutamatergic neurons were enhanced in animal models of conditional fear, which involved a mechanism wherein the projections of ventrolateral periaqueductal gray glutamatergic neurons to the rostral ventromedial medulla were enhanced.<sup>25</sup> Indeed, ventrolateral periaqueductal gray neurons receive major inputs from numerous brain regions involved in the stress response.<sup>25,67,68</sup> We thus would like to point out that, although the ventrolateral periaqueductal gray is a common region involved in the pathophysiology of pain, cell type–specific regulation of the tone of the central amygdala–ventrolateral periaqueductal gray circuit could be one of the factors involved in the development of treatment-resistant depression, including depression with pain. In addition, although the central amygdala–periaqueductal gray pathway contributes to multiple behavioral outputs,<sup>25,37,67</sup> the specific projection of this circuit to the ventrolateral periaqueductal gray glutamatergic neurons could be relatively more important for the nociception in current animal models.

Excitingly, cell type–specific manipulations of the activity of the central amygdala–ventrolateral periaqueductal gray circuit can effectively alleviate nociception in a mouse model of depression. The significance of these findings, with respect to treatment-resistant pain, is that manipulations targeting this neural circuitry would have effects on pain symptoms. As pharmacologic options for the treatment of pain in depression remain quite limited, these findings raise the possibility of developing optimal treatments that involve nondrug

approaches, such as deep brain stimulation or transcranial magnetic stimulation,<sup>69,70</sup> to target the converging pathways.

## Acknowledgments

The authors thank Xiang Yu, Ph.D. (Institute of Neuroscience, Chinese Academy of Sciences, Shanghai, China), for providing Ai9 mice, Guoqiang Bi, Ph.D. (School of Life Sciences, University of Science and Technology of China, Hefei, China), for providing c-fos-tTA mice, and Fu-Qiang Xu, Ph.D. (Wuhan Institute of Physics and Mathematics, Chinese Academy of Sciences, Wuhan, China), and Tian Xue, Ph.D. (School of Life Sciences, University of Science and Technology of China, Hefei, China), for technical support.

## Research Support

Support was provided from the National Natural Science Foundation of China (Beijing, China; 81870877, 91732303, and 91849119), and the National Key Research and Development Program of China (Beijing, China; 2016YFC1305900).

## Competing Interests

The authors declare no competing interests.

## Correspondence

Address correspondence to Dr. Zhang: Hefei National Laboratory for Physical Sciences at the Microscale, Department of Biophysics and Neurobiology, University of Science and Technology of China, Hefei, Anhui 230027, China. zhizhang@ustc.edu.cn. This article may be accessed for personal use at no charge through the Journal Web site, [www.anesthesiology.org](http://www.anesthesiology.org).

## References

1. Bair MJ, Robinson RL, Katon W, Kroenke K: Depression and pain comorbidity: A literature review. *Arch Intern Med* 2003; 163:2433–45
2. Nekovarova T, Yamamotova A, Vales K, Stuchlik A, Fricova J, Rokyta R: Common mechanisms of pain and depression: Are antidepressants also analgesics? *Frontiers in behavioral neuroscience* 2014; 8:1–12
3. Torta RG, Munari J: Symptom cluster: Depression and pain. *Surg Oncol* 2010; 19:155–9
4. Vitaly N, Lauren LC, Kyungmo P, Sawsan AS, Clauw DJ, Harris RE: Intrinsic brain connectivity in fibromyalgia is associated with chronic pain intensity. *Arthritis Rheum* 2014; 62:2545–55
5. Guo W, Feng L, Xue Z, Gao K, Liu Z, Xiao C, Chen H, Zhao J: Abnormal resting-state cerebellar–cerebral functional connectivity in treatment-resistant depression and treatment sensitive depression. *Progr Neuropsychopharmacol Biol Psychiatry* 2013; 44:51–7

6. Kim H, Chen L, Lim G, Sung B, Wang S, McCabe MF, Rusanescu G, Yang L, Tian Y, Mao J: Brain indoleamine 2,3-dioxygenase contributes to the comorbidity of pain and depression. *J Clin Invest* 2012; 122:2940–54
7. Raison CL, Borisov AS, Majer M, Drake DE, Pagnoni G, Woolwine BJ, Vogt GJ, Massung B, Miller AH: Activation of central nervous system inflammatory pathways by interferon- $\alpha$ : Relationship to monoamines and depression. *Biol Psychiatry* 2009; 65:296–303
8. Müller N, Schwarz MJ: The immune-mediated alteration of serotonin and glutamate: Towards an integrated view of depression. *Mol Psychiatry* 2007; 12:988–1000
9. Berton O, McClung CA, Dileone RJ, Krishnan V, Renthal W, Russo SJ, Graham D, Tsankova NM, Bolanos CA, Rios M, Monteggia LM, Self DW, Nestler EJ: Essential role of BDNF in the mesolimbic dopamine pathway in social defeat stress. *Science* 2006; 311:864–8
10. Geng SJ, Liao FF, Dang WH, Ding X, Liu XD, Cai J, Han JS, Wan Y, Xing GG: Contribution of the spinal cord BDNF to the development of neuropathic pain by activation of the NR2B-containing NMDA receptors in rats with spinal nerve ligation. *Exp Neurol* 2010; 222:256–66
11. Martin KP, Wellman CL: NMDA receptor blockade alters stress-induced dendritic remodeling in medial prefrontal cortex. *Cerebral Cortex* 2011; 21: 2366–73
12. Nagata K, Imai T, Yamashita T, Tsuda M, Tozakisaitoh H, Inoue K: Antidepressants inhibit P2X<sub>4</sub> receptor function: A possible involvement in neuropathic pain relief. *Molecular Pain* 2009; 5:1–12
13. Linnman C, Beucke J-C, Jensen KB, Gollub RL, Kong J: Sex similarities and differences in pain-related periaqueductal gray connectivity. *Pain* 2012; 153:444–54
14. Apkarian AV, Bushnell MC, Treede RD, Zubieta JK: Human brain mechanisms of pain perception and regulation in health and disease. *Eur J Pain* 2005; 9:463–84
15. Tracey I, Mantyh PW: The cerebral signature for pain perception and its modulation. *Neuron* 2007; 55:377–91
16. Han S, Soleiman MT, Soden ME, Zweifel LS, Palmiter RD: Elucidating an affective pain circuit that creates a threat memory. *Cell* 2015; 162:363–74
17. Wang GQ, Cen C, Li C, Cao S, Wang N, Zhou Z, Liu XM, Xu Y, Tian NX, Zhang Y, Wang J, Wang LP, Wang Y: Deactivation of excitatory neurons in the prelimbic cortex via Cdk5 promotes pain sensation and anxiety. *Nat Commun* 2015; 6:7660
18. Nakajima K, Obata H, Iriuchijima N, Saito S: An increase in spinal cord noradrenaline is a major contributor to the antihyperalgesic effect of antidepressants after peripheral nerve injury in the rat. *Pain* 2012; 153:990–7
19. Rush AJ, Trivedi MH, Wisniewski SR, Nierenberg AA, Stewart JW, Diane W, George N, Thase ME, Lavori PW, Lebowitz BD: Acute and longer-term outcomes in depressed outpatients requiring one or several treatment steps: A STAR\*D report. *Am J Psychiatry* 2006; 163:1905–17
20. Ferguson JM: SSRI antidepressant medications: Adverse effects and tolerability. *Prim Care Companion J Clin Psychiatry* 2001; 3:22–7
21. Hieronymus F, Emilsson JF, Nilsson S, Eriksson E: Consistent superiority of selective serotonin reuptake inhibitors over placebo in reducing depressed mood in patients with major depression. *Mol Psychiatry* 2016; 21:523–30
22. Wiech K, Tracey I: The influence of negative emotions on pain: Behavioral effects and neural mechanisms. *Neuroimage* 2009; 47:987–94
23. Xu C, Krabbe S, Gründemann J, Botta P, Fadok JP, Osakada F, Saur D, Grewe BF, Schnitzer MJ, Callaway EM, Lüthi A: Distinct hippocampal pathways mediate dissociable roles of context in memory retrieval. *Cell* 2016; 167:961–72.e16
24. Cai Y-Q, Wang W, Paulucci-Holthauzen A, Pan ZZ: Brain circuits mediating opposing effects on emotion and pain. *J Neurosci* 2018; 38:6340–9
25. Tovote P, Esposito MS, Botta P, Chaudun F, Fadok JP, Markovic M, Wolff SB, Ramakrishnan C, Fenno L, Deisseroth K: Midbrain circuits for defensive behaviour. *Nature* 2016; 534:206–12
26. Rosso IM, Cintron CM, Steingard RJ, Renshaw PF, Young AD, Yurgelun-Todd DA: Amygdala and hippocampus volumes in pediatric major depression. *Biol Psychiatry* 2005; 57:21–6
27. Diamond DM, Campbell A, Park CR, Vouimba RM: Preclinical research on stress, memory, and the brain in the development of pharmacotherapy for depression. *Eur Neuropsychopharmacol* 2004; 14(suppl 5):491–5
28. Robinson MJ, Edwards SE, Iyengar S, Bymaster F, Clark M, Katon W: Depression and pain. *Front Biosci (Landmark Ed)* 2009; 14:5031–51
29. Burgmer M, Gaubitz M, Konrad C, Wrenger M, Hilgart S, Heuft G, Pfleiderer B: Decreased gray matter volumes in the cingulo-frontal cortex and the amygdala in patients with fibromyalgia. *Psychosom Med* 2009; 71:566–73
30. Ji G, Sun H, Fu Y, Li Z, Pais-Vieira M, Galhardo V, Neugebauer V: Cognitive impairment in pain through amygdala-driven prefrontal cortical deactivation. *J Neurosci* 2010; 30:5451–64
31. Bushnell MC, Čeko M, Low LA: Cognitive and emotional control of pain and its disruption in chronic pain. *Nat Rev Neurosci* 2013; 14:502–11
32. Neugebauer V, Li W, Bird GC, Han JS: The amygdala and persistent pain. *Neuroscientist* 2004; 10:221–34
33. Gonçalves L, Silva R, Pinto-Ribeiro F, Pêgo JM, Bessa JM, Pertovaara A, Sousa N, Almeida A: Neuropathic pain is associated with depressive behaviour and

- induces neuroplasticity in the amygdala of the rat. *Exp Neurol* 2008; 213:48–56
34. Penzo MA, Robert V, Tucciarone J, De Bundel D, Wang M, Van Aelst L, Darvas M, Parada LF, Palmiter RD, He M: The paraventricular thalamus controls a central amygdala fear circuit. *Nature* 2015; 519:455–9
  35. Zhang Z, Cai YQ, Zou F, Bie B, Pan ZZ: Epigenetic suppression of GAD65 expression mediates persistent pain. *Nat Med* 2011; 17:1448–55
  36. Franklin KB, Paxinos G: *The Mouse Brain in Stereotaxic Coordinates*. New York, Academic Press, 2008
  37. Avegno EM, Lobell TD, Itoga CA, Baynes BB, Whitaker AM, Weera MM, Edwards S, Middleton JW, Gilpin NW: Central amygdala circuits mediate hyperalgesia in alcohol-dependent rats. *J Neurosci* 2018; 38:7761–73
  38. Oliveira MA, Prado WA: Role of PAG in the antinociception evoked from the medial or central amygdala in rats. *Brain Res Bull* 2001; 54:55–63
  39. Zingg B, Chou X-l, Zhang Z-g, Mesik L, Liang F, Tao HW, Zhang LI: AAV-mediated anterograde transsynaptic tagging: Mapping corticocollicular input-defined neural pathways for defense behaviors. *Neuron* 2017; 93:33–47
  40. Callaway EM, Luo L: Monosynaptic circuit tracing with glycoprotein-deleted rabies viruses. *J Neurosci* 2015; 35:8979–85
  41. Wickersham IR, Lyon DC, Barnard RJ, Mori T, Finke S, Conzelmann KK, Young JA, Callaway EM: Monosynaptic restriction of transsynaptic tracing from single, genetically targeted neurons. *Neuron* 2007; 53:639–47
  42. Ramirez S, Liu X, MacDonald CJ, Moffa A, Zhou J, Redondo RL, Tonegawa S: Activating positive memory engrams suppresses depression-like behaviour. *Nature* 2015; 522:335–9
  43. Christiansen SH, Olesen MV, Wörtwein G, Woldbye DP: Fluoxetine reverts chronic restraint stress-induced depression-like behaviour and increases neuropeptide Y and galanin expression in mice. *Behav Brain Res* 2011; 216:585–91
  44. Kim KS, Han PL: Optimization of chronic stress paradigms using anxiety- and depression-like behavioral parameters. *J Neurosci Res* 2006; 83:497–507
  45. François A, Low SA, Sypek EI, Christensen AJ, Sotoudeh C, Beier KT, Ramakrishnan C, Ritola KD, Sharif-Naeini R, Deisseroth K: A brainstem-spinal cord inhibitory circuit for mechanical pain modulation by GABA and enkephalins. *Neuron* 2017; 93:822–39
  46. Gamaro GD, Xavier MH, Denardin JD, Pilger JA, Ely DR, Ferreira MB, Dalmaz C: The effects of acute and repeated restraint stress on the nociceptive response in rats. *Physiol Behav* 1998; 63:693–7
  47. Liu X, Ramirez S, Redondo RL, Tonegawa S: Identification and manipulation of memory engram cells. *Cold Spring Harb Symp Quant Bio* 2014; 79:59–65
  48. Cadwell CR, Palasantza A, Jiang X, Berens P, Deng Q, Yilmaz M, Reimer J, Shen S, Bethge M, Tolias KF: Electrophysiological, transcriptomic and morphologic profiling of single neurons using Patch-seq. *Nat Biotechnol* 2016; 34:199–203
  49. Madisen L, Zwingman TA, Sunkin SM, Oh SW, Zariwala HA, Gu H, Ng LL, Palmiter RD, Hawrylycz MJ, Jones AR: A robust and high-throughput Cre reporting and characterization system for the whole mouse brain. *Nat Neurosci* 2010; 13:133–40
  50. Truini A, Tinelli E, Gerardi MC, Calistri V, Iannuccelli C, La Cesa S, Tarsitani L, Mainero C, Sarzi-Puttini P, Cruccu G, Caramia F, Di Franco M: Abnormal resting state functional connectivity of the periaqueductal grey in patients with fibromyalgia. *Clin Exp Rheumatol* 2016; 34(2 Suppl 96):S129–33
  51. Meier ML, Stämpfli P, Humphreys BK, Vrana A, Seifritz E, Schweinhardt P: The impact of pain-related fear on neural pathways of pain modulation in chronic low back pain. *Pain Rep* 2017; 2:601–5
  52. Qin W, Tian J, Bai L, Pan X, Yang L, Chen P, Dai J, Ai L, Zhao B, Gong Q: fMRI connectivity analysis of acupuncture effects on an amygdala-associated brain network. *Mol Pain* 2008; 4:1–17
  53. Aloisi AM, Ceccarelli I, Lupo C: Behavioural and hormonal effects of restraint stress and formalin test in male and female rats. *Brain Res Bull* 1998; 47:57–62
  54. Long CC, Sadler KE, Kolber BJ: Hormonal and molecular effects of restraint stress on formalin-induced pain-like behavior in male and female mice. *Physiol Behav* 2016; 165:278–85
  55. Galea LA, McEwen BS, Tanapat P, Deak T, Spencer RL, Dhabhar FS: Sex differences in dendritic atrophy of CA3 pyramidal neurons in response to chronic restraint stress. *Neuroscience* 1997; 81:689–97
  56. Zimmer C, Basler HD, Vedder H, Lautenbacher S: Sex differences in cortisol response to noxious stress. *Clin J Pain* 2003; 19:233–9
  57. Bulls HW, Freeman EL, Anderson AJ, Robbins MT, Ness TJ, Goodin BR: Sex differences in experimental measures of pain sensitivity and endogenous pain inhibition. *J Pain Res* 2015; 8:311–20
  58. Kurdi MS, Theerth KA, Deva RS: Ketamine: Current applications in anesthesia, pain, and critical care. *Anesth Essays Res* 2014; 8:283–90
  59. Dowben JS, Grant JS, Keltner NL: Biological perspectives: Ketamine as an alternative treatment for treatment-resistant depression. *Perspect Psychiatr Care* 2013; 49:2–4

60. Murrough JW, Iosifescu DV, Chang LC, Al Jurdi RK, Green CE, Perez AM, Iqbal S, Pillemer S, Foulkes A, Shah A, Charney DS, Mathew SJ: Antidepressant efficacy of ketamine in treatment-resistant major depression: a two-site randomized controlled trial. *Am J Psychiatry* 2013; 170:1134–42
61. Hocking G, Cousins MJ: Ketamine in chronic pain management: An evidence-based review. *Anesth Analg* 2003; 97:1730–9
62. Tang J, Xue W, Xia B, Ren L, Tao W, Chen C, Zhang H, Wu R, Wang Q, Wu H, Duan J, Chen G: Involvement of normalized NMDA receptor and mTOR-related signaling in rapid antidepressant effects of Yueju and ketamine on chronically stressed mice. *Sci Rep* 2015; 5:13573
63. Zhang JC, Li SX, Hashimoto K: R (–)-ketamine shows greater potency and longer lasting antidepressant effects than S (+)-ketamine. *Pharmacol Biochem Behav* 2014; 116:137–41
64. Jing W, Yossef G, Duo X, Tukey DS, Shamir DB, Eberle SE, Zou AH, Blanck TJJ, Ziff EB: A single subanesthetic dose of ketamine relieves depression-like behaviors induced by neuropathic pain in rats. *ANESTHESIOLOGY* 2011; 115:812–21
65. Marks DM, Shah MJ, Patkar AA, Masand PS, Park GY, Pae CU: Serotonin-norepinephrine reuptake inhibitors for pain control: premise and promise. *Curr Neuropharmacol* 2009; 7:331–6
66. Basbaum AI, Bautista DM, Scherrer G, Julius D: Cellular and molecular mechanisms of pain. *Cell* 2009; 139:267–84
67. Ozawa T, Ycu EA, Kumar A, Yeh LF, Ahmed T, Koivumaa J, Johansen JP: A feedback neural circuit for calibrating aversive memory strength. *Nat Neurosci* 2017; 20:90–7
68. Li Y, Zeng J, Zhang J, Yue C, Zhong W, Liu Z, Feng Q, Luo M: Hypothalamic Circuits for Predation and Evasion. *Neuron* 2018; 97:911–24.e5
69. Pascual-Leone A, Rubio B, Pallardó F, Catalá MD: Rapid-rate transcranial magnetic stimulation of left dorsolateral prefrontal cortex in drug-resistant depression. *Lancet* 1996; 348:233–7
70. Taghva AS, Malone DA, Rezai AR: Deep brain stimulation for treatment-resistant depression. *World Neurosurg* 2013; 80:S27.e17–24